COMPTON HEATED WINDS AND CORONAE ABOVE ACCRETION DISKS.
I. DYNAMICS

MITCHELL C. BEGELMAN,[1,2] CHRISTOPHER F. MCKEE,[1,3] AND GREGORY A. SHIELDS[4,5]

ABSTRACT

X-rays emitted in the inner part of an accretion disk system can heat the surface of the disk farther out, producing a corona and possibly driving off a strong wind. We analyze the dynamics of Compton-heated coronae and winds, using an approximate two-dimensional technique to estimate the mass loss rate as a function of distance from the source of X-rays.

Our findings have important dynamical implications for accretion disks in quasars, active galactic nuclei, X-ray binaries, and cataclysmic variables. These include: (1) mass loss from the disk possibly comparable with or exceeding the net accretion rate onto the central compact object, which may lead to unstable accretion; (2) sufficient angular momentum loss in some cases to truncate the disk in a semidetached binary at a smaller radius than that predicted by tidal truncation theories; and (3) combined static plus ram pressure in the wind adequate to confine line-emitting clouds in quasars and Seyfert galaxies.

We analyze and discuss the observable manifestations of Compton-heated winds and coronae in a companion paper (Paper II).

Subject headings: galaxies: Seyfert — hydrodynamics — quasars — stars: accretion —
X-rays: binaries

I. INTRODUCTION

Coronae and winds form outside the photospheres of stars when energy from the stellar interior is deposited in gas which is too tenuous to radiate it away efficiently. Viscous accretion disks also have internal heat sources and densities which decline sharply away from the equatorial plane; hence coronae and winds may develop in much the same way (Liang and Price 1977). Several mechanisms have been proposed for internally powering coronae and winds from disks, including acoustic fluxes driven by convection (Bisnovatyi-Kogan and Blinnikov 1977; Livio and Shaviv 1981), turbulence (Icke 1976), or gravitational instabilities (Paczyński 1978); and nonthermal heating by magnetic flares (Galeev, Rosner, and Vaiana 1979). In addition to various forms of heating from within, the outer parts of an accretion disk may intercept some of the energetic radiation emitted in the inner parts of the gas flow which surrounds the central compact object (Shakura and Sunyaev 1973). The flux of radiation produced in the central regions of the accretion disk and absorbed at some larger radius may greatly exceed the heating produced locally. The rate of heating per particle is proportional to the intensity of radiation, while the cooling rate in the disk relies on two-particle processes and therefore declines with the density as one moves away from the equatorial plane of the disk. Below some critical density, radiative heating

and cooling processes overwhelm two-body cooling, and the gas heats toward some high temperature determined by interactions between the particles and the photons. For X-ray binaries and quasars, the radiation is sufficiently hard that the gas can be heated to temperatures exceeding 10^7 K, predominantly through the Compton process. Since these temperatures far exceed the internal temperatures associated with the outer parts of accretion disks, the heated gas forms a tenuous corona with a thickness exceeding that of the disk. If the sound speed in the heated gas also exceeds the escape speed from the system at the radius of interest, then the gas steadily escapes as it is heated and a wind results.

Our purpose in this paper is to analyze the dynamics of Compton-heated winds and coronae that may form above accretion disks whose surfaces are irradiated by X-rays from a compact central source. Parts of this and related problems have been tackled by other authors, and we extend or complement their work. For example, Compton-heated winds from stars have been studied extensively, for the conditions appropriate to X-ray binaries like HZ Her. Here the main motivation has been to discover whether mass transfer from the "normal" star to the compact companion could be "self-excited" (Davidson and Ostriker 1973; Arons 1973; London, McCray, and Auer 1981 and references therein; London and Flannery 1982) by X-ray irradiation of the former by the latter. We examine the dynamical implications of Compton-driven mass loss from disks in § IV, and find that mass *and* angular momentum loss can have an important impact on both the structure of the disk and the evolution of an X-ray binary. We defer our

70

analysis of the directly observable manifestations of Compton-heated winds and coronae to a companion paper (Begelman and McKee 1983, Paper II). These depend sensitively on the geometry of the disk and the transfer of incident X-rays through the heated gas, whereas the purely dynamical features of the mass loss do not.

In order to make our quantitative analysis tractable, we have made a number of simplifying assumptions:

i) We consider heating and cooling by Compton scattering only. London, McCray, and Auer (1981) have demonstrated that our neglect of line cooling on the dynamics is justified, provided the gas heats to temperatures greater than a few times 10^6 K over a pressure scale height. This is probably the case for the spectra and dimensions appropriate to quasars and X-ray binaries, but may not apply to objects with much softer spectra.

ii) We assume that the disk photosphere is irradiated by a point source of X-rays located at the center of the disk. The disk is likely to be opaque to all but the most energetic X- and gamma-rays, but particles at the photosphere will be able to "see" the central source if the disk flares, i.e., if the height of the photosphere above the equatorial plane increases with radius R at a rate faster than one proportional to R. Shakura and Sunyaev (1973) found that the outer regions of their disk models flared, and foresaw that Compton-heated winds and coronae could result. Other geometric configurations may enable hard radiation from the inner regions to reach the outer parts of the disk, e.g., if the source of X-rays extends far enough above and below the equatorial plane that its thickness exceeds that of the disk, or if radiation from a central compact source is scattered down onto the disk by material lying at high latitudes. Provided the local radiation intensity at the disk photosphere can be estimated self-consistently, the local properties of the resulting wind or coronae can be inferred.

iii) We neglect nonthermal sources of energy from within the disk which may contribute to heating the corona or wind.

iv) We assume that conduction effects are not important, except perhaps in a thin boundary layer near the base of the corona/wind. This contrasts with the nonthermal, conduction-stabilized corona considered by Liang and Thompson (1979). In a Compton-heated corona, conduction is less important because (1) temperatures are lower than a few times 10^8 K, (2) densities are higher than in the nonthermal case, and (3) the heating is spread throughout the corona/wind. It is interesting to contrast the third point with coronae or winds driven from below, where it is often argued that most of the energy is dumped into a narrow layer at the base, and further redistribution relies largely on conduction.

v) We assume that the X-ray source is time-independent. Thus, caution should be exercised in applying our results to pulsating or highly variable sources, although it may be permissible to use a time-averaged luminosity if the variability time scale is shorter than the characteristic dynamical time at the radius of interest.

vi) We neglect the effects of radiation pressure. Where attenuation is unimportant, this can be remedied by replacing the central mass by an effective mass, smaller by a factor $(1 - L/L_E)$, where L_E is the Eddington limit and L is the luminosity of the source. However, where attenuation along the line of sight is significant, the required modifications are much more complicated. It is worth noting that the characteristic "critical" luminosity in our problem (eq. [2.12]) is typically a few percent of L_E or less, so that strong Compton-heated winds and coronae do not require luminosities close to the Eddington limit.

vii) We consider only the gravitational field of the central compact object in analyzing the structure and dynamics of the corona/wind. In particular, we neglect the self-gravity of the disk and the distributed mass of a star cluster, both of which may be important in quasars, and we also neglect the gravitational influence of a binary companion, which may influence the outer corona/wind in X-ray binaries.

viii) We seek solutions for the corona/wind in which the pressure approaches zero away from the disk. Thus, we ignore possible back-pressure due to a high-latitude wind (jet?) or, in the case of an X-ray binary, a wind from the companion star.

We proceed as follows. In § II we review the thermal properties of gas irradiated by X-rays, give the relevant heating and cooling rates, and describe the qualitative behavior of Compton-heated winds and coronae. For a central radiation source, the structure of the corona/wind can be divided into five regions, the boundaries between which depend on radius and on the luminosity and spectrum of the X-ray source. This parameter space is summarized in Figure 1. In § III we analyze optically thin Compton-heated winds in detail, and derive expressions for the local mass loss rate in each region of the parameter space. An analysis of radiative transfer effects is deferred to Paper II, but the results of this section are readily generalized to optically thick winds. The integrated losses of mass and angular momentum due to Compton-heated winds are computed in § IV, for a disk of finite extent. We find that the total mass loss may greatly exceed the accretion rate responsible for producing the X-ray flux, and demonstrate that this situation may lead to instability in the accretion flow, and a fluctuating luminosity. The angular momentum carried away by the wind is also substantial, and will in some cases be able to truncate the accretion disk in an X-ray binary at a smaller radius than that predicted by the tidal truncation theory of Smak (1976) and Paczyński (1977).

II. GENERAL CONSIDERATIONS

a) Thermal Equilibrium

The thermal equilibrium of a gas exposed to ionizing radiation which extends into the X-ray region of the spectrum has been calculated most recently by Krolik,

McKee, and Tarter (1981, hereafter KMT) for conditions appropriate to quasars and by London, McCray, and Auer (1981) for the higher density conditions expected in binary X-ray sources. The thermal state of the gas is determined by the shape of the spectrum together with the parameter

$$\Xi' = \frac{4\pi J}{pc} , \qquad (2.1)$$

where J is the mean intensity of the radiation integrated over frequency and p is the gas pressure. For a beam of radiation, $4\pi J$ equals the flux F, and Ξ' is simply the ratio of the radiation pressure to the gas pressure. For a fully ionized gas of cosmic abundances, this parameter is related to the parameter Ξ used by KMT by the relation $\Xi' = (J/2.3J^{\text{ion}})\Xi$, where J^{ion} is the mean intensity of the ionizing radiation between 1 and 10^3 rydbergs.

For spectra appropriate to quasars or X-ray sources, there are two stable phases:

1. For $\Xi' < \Xi'_{c,\text{max}}$ there is a cool phase with $T \lesssim 10^{4.5}$ K, in which photoionization heating is balanced by recombination and line cooling. KMT assumed the density was sufficiently low ($n_e \lesssim 10^{12}$ cm^{-3}) that line cooling was effective and found $\Xi'_{c,\text{max}} = (2.5-10)(J/J^{\text{ion}})$ for a variety of power law spectra. London, McCray, and Auer (1981) assumed that line cooling was collisionally quenched and found $\Xi'_{c,\text{max}} \approx \frac{1}{2}-4$ for a variety of bremsstrahlung-like spectra.

2. For $\Xi' > \Xi'_{h,\text{min}}$ there is a hot phase in which Compton heating by energetic photons is balanced by inverse Compton cooling by softer photons. The equilibrium temperature T_h is generally close to the "inverse Compton temperature" $T_{\text{IC}} \approx 10^8$ K, discussed below. The value of $\Xi'_{h,\text{min}}$ is determined by the effect of other heating and cooling processes; if the only such process which is important is bremsstrahlung, then KMT showed

$$\Xi'_{h,\text{min}} = 1.2 T_{\text{IC8}}^{-3/2} , \qquad (2.2)$$

where $T_{\text{IC8}} = T_{\text{IC}}/10^8$ K.

For sufficiently hard ionizing continua, there is a small range $\Xi'_{h,\text{min}} \lesssim \Xi' \lesssim \Xi'_{c,\text{max}}$ in which the hot and cool phases can exist in pressure equilibrium with each other. In this range of Ξ' there is also an intermediate equilibrium temperature that is thermally unstable. On the other hand, for softer continua giving $T_h \lesssim 10^7$ K, the equilibrium temperature is a steep but monotonic function of Ξ in the range $\Xi = 10^{\pm 1}$, and no two-phase equilibrium is possible.

The thermal equilibrium in the cool phase is a complicated function of atomic heating and cooling parameters, but fortunately that of the hot phase is much simpler (cf. KMT). For our applications, the size of the region producing most of the hard radiation is small compared to the volume of hot gas. If the gas is optically thin, then an isotropic source of radiation of luminosity L leads to heating and cooling rates per unit volume at a radius R of

$$n_e \Gamma = n_e \sigma_{\text{T}} \frac{\langle \epsilon \rangle}{m_e c^2} \frac{L}{4\pi R^2} , \qquad (2.3a)$$

$$n^2 \Lambda_{\text{IC}} = n_e \sigma_{\text{T}} \frac{4kT}{m_e c^2} \frac{L}{4\pi R^2} . \qquad (2.3b)$$

where

$$\langle \epsilon \rangle = L^{-1} \int_0^\infty h\nu L_\nu \, d\nu .$$

In the hot phase, the temperature rises until inverse Compton cooling, which predominates, balances Compton heating. This gives an equilibrium temperature

$$kT_{\text{IC}} = \tfrac{1}{4}\langle \epsilon \rangle , \qquad (2.4)$$

which allows us to reexpress the heating rate as

$$\Gamma = \frac{kT_{\text{IC}}}{m_e c^2} \frac{\sigma_{\text{T}} L}{\pi R^2} . \qquad (2.5)$$

b) Qualitative Behavior of Compton-heated Winds

An accretion disk is thin at radius R_0 if its internal sound speed is much smaller than the local Keplerian speed. The vertical scale height h'_d is related to R_0 through the ratio of these two speeds (Shakura and Sunyaev 1973). At larger distances from the midplane the pressure and density both drop sharply. If such a disk is illuminated by X-ray and EUV continuum, the ionization parameter Ξ will increase rapidly with increasing height in the atmosphere, eventually exceeding $\Xi_{c,\text{max}}$. Above this level, the gas must either be in the hot phase, $T = T_{\text{IC}}$, or be in the process of heating toward T_{IC}.

A nearly hydrostatic corona will exist at R_0 if the Compton temperature T_{IC} is less than the "escape temperature" $T_g \equiv GM\mu/R_0 k$, that is,

$$\frac{T_{\text{IC}}}{T_g} = \frac{c_{\text{IC}}^2}{v_g^2} < 1 \qquad (2.6)$$

where $c_{\text{IC}} = (kT_{\text{IC}}/\mu)^{1/2}$ is the isothermal sound speed at T_{IC} and v_g is the Keplerian velocity. This condition is satisfied inside the radius

$$R_{\text{IC}} \equiv \frac{GM\mu}{kT_{\text{IC}}} = \frac{1.0 \times 10^{10}}{T_{\text{IC8}}} \left(\frac{M}{M_\odot}\right) \text{cm} . \qquad (2.7)$$

Therefore, for

$$\xi \equiv R_0/R_{\text{IC}} = T_{\text{IC}}/T_g \qquad (2.8)$$

much less than one, we expect a sharp transition from a disk photosphere (or photoionized chromosphere) to a static hot corona at $T = T_{\text{IC}}$. On the other hand, for $\xi > 1$, a vigorous wind may arise as gas rising above the level at which $\Xi = \Xi_{c,\text{max}}$ is heated to a temperature that exceeds the escape temperature; we term this the "wind region" of the disk. In fact, the analysis in § III shows that a significant wind occurs for $\xi \gtrsim 0.1$. A wind is possible only at large radii because the Compton temperature T_{IC} depends on the spectrum of the radiation and not on its intensity, whereas T_g decreases with increasing R_0.

In the wind region, the finite heating rate of the hot gas must be considered. Conceivably, the gas will not

have time to heat to $T_{\rm IC}$ before it has reached height $\sim R_0$ above the disk. In this case, the effectiveness of gravity at inhibiting the wind is a function of the temperature actually reached by the gas at heights $\sim R_0$, compared with T_g. This motivates the definition of a "characteristic temperature," $T_{\rm ch}$, that satisfies the self-consistent condition $kT_{\rm ch} = \Gamma_0(R_0/c_{\rm ch})$, where Γ_0 is the optically thin heating rate evaluated at R_0 and $c_{\rm ch} = (kT_{\rm ch}/\mu)^{1/2}$ is the isothermal sound speed at $T_{\rm ch}$. This gives

$$kT_{\rm ch} = \mu^{1/3}(\Gamma_0 R_0)^{2/3} . \qquad (2.9)$$

The importance of gravity in the wind region may be expressed in terms of the dimensionless parameter

$$\alpha \equiv \frac{t_g}{t_h(T_{\rm ch})} = \left(\frac{T_{\rm ch}}{T_g}\right)^{1/2} , \qquad (2.10)$$

where $t_g \equiv R_0/v_g$ and $t_h(T_{\rm ch}) \equiv kT_{\rm ch}/\Gamma_0$ are characteristic gravitational and heating time scales. For $\alpha > 1$ and $\xi = R_0/R_{\rm IC} > 1$, the wind heats quickly enough to escape without suffering a large pressure drop due to gravity. We denote the radius at which $\alpha = 1$ as $R_{\rm ch}$; for $R_0 > {\rm Max}\,(R_{\rm ch}, R_{\rm IC})$, gravity does not inhibit the wind. Equations (2.9) and (2.10) together with the definition of T_g imply

$$R_{\rm ch} = \alpha^{-6}R_{\rm IC} . \qquad (2.11)$$

The condition that the three temperatures $T_{\rm IC}$, T_g, and $T_{\rm ch}$ all be equal implies that $\xi = 1$ and $\alpha = 1$. This defines a critical luminosity

$$L_{\rm cr} = \frac{1}{8}\left(\frac{m_e}{\mu}\right)^{1/2}\left(\frac{m_e c^2}{kT_{\rm IC}}\right)^{1/2}L_E \qquad (2.12a)$$

$$= 0.030\,T_{\rm IC8}^{-1/2}L_E , \qquad (2.12b)$$

where

$$L_E = 4\pi GM\mu_e c/\sigma_T \approx 8\pi ckT_{\rm IC}R_{\rm IC}/\sigma_T$$

$$= 1.5 \times 10^{38}(M/M_\odot)\ {\rm ergs\ s}^{-1} \qquad (2.12c)$$

is the Eddington luminosity, and $\mu_e \approx 2\mu$ is the mean mass per electron. Note that $L_{\rm cr}$ is an intrinsic function of the continuum source, involving M and $T_{\rm IC}$; it is independent of R_0. One may readily show that

$$\alpha^2 = \frac{T_{\rm ch}}{T_g} = \left(\frac{L}{L_{\rm cr}}\right)^{2/3}\xi^{1/3} , \qquad (2.13)$$

$$\frac{T_{\rm IC}}{T_{\rm ch}} = \left(\frac{L}{L_{\rm cr}}\right)^{-2/3}\xi^{2/3} . \qquad (2.14)$$

Hence, if $L > L_{\rm cr}$, then gravity is not important ($\alpha > 1$) anywhere in the wind region ($T_{\rm IC} > T_g, \xi > 1$). Evidently, $L/L_{\rm cr}$ characterizes the effectiveness of the X-ray luminosity in overcoming gravity, not by radiation pressure as in the ordinary Eddington limit, but by Compton heating. For $T_{\rm IC} \gtrsim 10^7$ K, one has $L_{\rm cr} < 0.1L_E$, and our neglect of radiation pressure is self-consistent.

Our description of the disk is completed by intro-

ducing a third radius, $R_{\rm iso}$, at which $T_{\rm IC} = T_{\rm ch}$. In terms of $L/L_{\rm cr}$ one has

$$\frac{R_{\rm iso}}{R_{\rm IC}} = \frac{L}{L_{\rm cr}} = \left(\frac{R_{\rm IC}}{R_{\rm ch}}\right)^{1/2} . \qquad (2.15)$$

Figure 1 illustrates the various possibilities as a function of luminosity, Compton temperature, and location in the disk. The left half of the diagram corresponds to radii inside $R_{\rm IC}$, where there is a bound corona at temperature $T_{\rm IC}$; for $R < 0.1R_{\rm IC}$ the mass loss rate is exponentially small. The right half corresponds to the wind region. It is worth noting here that the boundaries of the wind zones A–C are insensitive to radiative transfer effects. Most of the heating in these zones occurs at heights $\sim R_0$ above the disk, where the optical depth along the line of sight to the X-ray source can be shown to be small (Paper II). Of course, the division between corona and wind depends only on the spectrum of the radiation, not on its intensity; hence it is never affected by Thomson scattering along the line of sight.

The mass loss rate per unit area in each region of the graph is analyzed in detail in § III. There we show that the functional form of $\dot m$ depends on $L/L_{\rm cr}$ and ξ, whereas the magnitude of $\dot m$ is determined by the pressure p_0 at the point in the atmosphere where rapid heating begins. As just mentioned, the functional form of $\dot m$ is insensitive to radiative transfer; however, the magnitude does depend directly on the attenuation of the radiation between the source and the disk surface
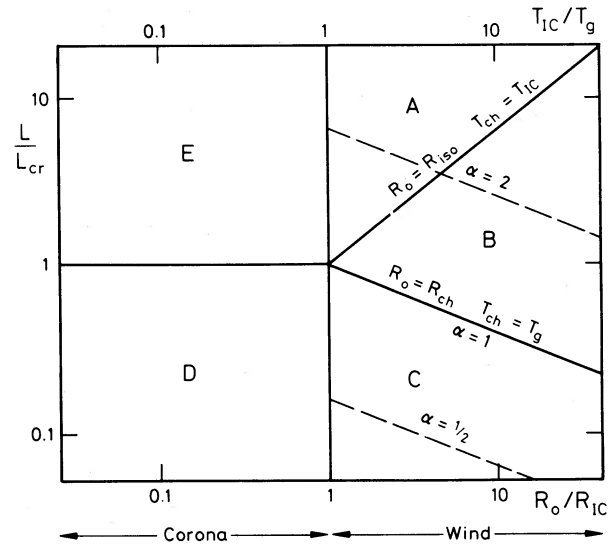

FIG. 1.—Parameter space for Compton-heated winds from accretion disks. The radius R_0 at which a streamline originates on the surface of the disk is normalized to $R_{\rm IC}$, the radius at which gas at the Compton temperature $T_{\rm IC}$ is marginally bound. The parameter $L/L_{\rm cr}$, where $L_{\rm cr} = 0.03\,T_{\rm IC8}^{-1/2}L_E$, measures the effectiveness of the luminosity in driving a wind by Compton heating. The outer part of the disk, comprising Regions A–C, is the wind region in which gas at $T_{\rm IC}$ is unbound ($\xi \equiv R_0/R_{\rm IC} > 1$). In the inner part of the disk (Regions D and E) is a quasi-static corona with a negligible mass loss rate for $\xi \lesssim 0.1$.

(Paper II). The essential results of the analysis in § III may be summarized as follows:

Region A.—Here $T_g < T_{IC} < T_{ch}$, so that gas at T_{IC} is not bound to the disk, and gas flowing through the base of the corona at $\Xi' = \Xi'_{c,max}$ is heated to $T \approx T_{IC}$ before it reaches a height $\sim R_0$ above the disk. This is possible in an annulus $1 < \zeta < R_{iso}/R_{IC} = L/L_{cr} < 30T_{IC8}^{-1/2}$, where the last inequality follows from the requirement $L < L_E$. In § IIIe we show that this flow leaves the disk moving nearly in a plane-parallel fashion and passes through an isothermal sonic point $v^2 = c_s^2$ at a height much less than R_0 where T first approaches T_{IC}. The gas further accelerates to reach a critical point $v^2 = (5/3)c_s^2$ at a height $\sim R_0$ above the disk, by which point the flow has become roughly spherical. The mass loss rate per unit area is given by $\dot{m} \approx (\frac{1}{2})p_0/c_{IC}$.

Region B.—Here $T_g < T_{ch} < T_{IC}$, so that the gas reaches $T \sim T_{ch}$ at a height $\sim R_0$, but this suffices to overcome gravity. The temperature rises steadily as the flow rises above the disk and passes through a critical point at a height $\sim R_0$. The mass loss rate is of order $\dot{m} \approx p_0/c_{ch}$. If the disk extends to radii beyond Max (R_{iso}, R_{ch}), then the outer part of the disk will be in Region B.

Region C.—Here $T_{ch} < T_g < T_{IC}$ and $1 < \zeta < R_{ch}/R_{IC} = (L_{cr}/L)^2$. Gravity strongly retards the flow, and the velocity is regulated to a low value that allows the temperature to reach $\sim T_g$ at a height $\sim R_0$. At this point the flow is still subsonic, $v/c_s \ll 1$. The sonic point is reached only at much larger radii, $R_{sonic} \approx R_{ch} = \alpha^{-6}R_0$, where adiabatic cooling lowers c_s below the essentially constant flow velocity v. For $R_0 \ll R_{ch}$, one has $\alpha \ll 1$ and the pressure drop caused by gravity leads to a very low mass loss rate $\dot{m} \approx 6\alpha^4 p_0/c_{ch}$.

Region D.—Since $\zeta < 1$ and $L < L_{cr}$, this corresponds to a weakly heated corona. Gravity is strong enough to reduce mass loss by an exponential factor, $\dot{m} \propto \exp(-T_g/2T_{IC})$. The critical point occurs far from the disk $(R_{crit} \sim R_{ch} = \alpha^{-6}R_0)$ just as in Region C; however, the flow velocity is low enough that the heating is able to maintain $T \sim T_{IC}$ out to a radius of order $(T_g/T_{IC})R_0 < R_{crit}$.

Region E.—Here $\zeta < 1$ and $L > L_{cr}$ so that the corona is strongly heated. For a given value of $T_{IC}/T_g = \zeta$, the mass loss rate is similar to that in region D, evaluated at $L = L_{cr}$. The isothermal sonic point occurs at $r_1 \approx (\frac{1}{2})R_0(T_g/T_{IC}) < R_{ch}$. The heating in this case is strong enough to maintain $T \sim T_{IC}$ out to radii in excess of r_1.

These results are derived in § III by means of detailed analytic solutions of the hydrodynamic equations. The reader interested in the observational applications may skip to § IIIf, where we summarize the main quantitative results, and continue on to our discussion of dynamical applications in § IV.

III. THEORY OF OPTICALLY THIN COMPTON-HEATED WINDS

a) Basics

In analyzing outflow from a disk, we can either search for an exact similarity solution to an idealized problem or we can obtain approximate solutions for more realistic, non–self-similar problems. Bardeen and Berger (1978) have found a similarity solution for an infinite disk in our Region C, where the temperature of the wind scales as R_0^{-1}. We wish to determine the mass loss near the edge of the disk as well as in the interior, and for all of the regions discussed in § II; hence we shall develop an approximate, one-dimensional model for the outflow. Near the surface of the disk the flow is nearly plane-parallel, while farther out the streamlines diverge due to transverse gradients (and second derivatives) of pressure, gravity, and angular momentum, and eventually become radial. A certain amount of divergence is necessary for the existence of a sonic (critical) point, as we shall see in § IIIc. Interaction between flows arising from different radii is ignored; study of such effects would require two-dimensional numerical calculations.

Suppose we consider hydrodynamic variables to be functions of R_0, the radius of the disk at the base of a given streamline, and $r - R_0$, the distance along a streamline from the base. In terms of the dimensionless coordinate

$$y \equiv r/R_0 \,, \tag{3.1}$$

the divergence of streamlines can be characterized by a dimensionless flow tube area, normalized to unity at the base of the flow ($y = 1$):

$$A(y) \equiv y^{\langle \beta \rangle} \,. \tag{3.2}$$

Here $\langle \beta \rangle$ is the log-weighted average, between 1 and y, of the local rate of divergence

$$\beta(y) \equiv \frac{d \ln A}{d \ln y} \,. \tag{3.3}$$

We treat $\beta(y)$ as an unknown function constrained to vary between 0 at $y = 1$ (vertical flow) and ~ 2 at $y \gg 1$ (spherical flow). In terms of equation (3.1), the continuity equation can be written

$$\dot{m} = \rho v y^{\langle \beta \rangle} = \text{constant} \,, \tag{3.4}$$

where ρ and v are, respectively, density and velocity along a streamline. We shall demonstrate that although $\beta(y)$ is uncertain, the mass loss rate $\dot{m}$ is reasonably well determined.

The equation of motion along a streamline is given by

$$\rho v \frac{dv}{dr} = -\frac{dp}{dr} - \rho g(r) \,, \tag{3.5}$$

where $g(r)$ is the component of effective gravity (gravity plus centrifugal force) parallel to the streamline. Since the disk is assumed to be Keplerian and thin, $g(R_0) \ll g(2R_0)$. Rigorously, $g(r)$ depends on the streamline's trajectory, which is not known *a priori* even if $\beta(y)$ is specified. For example, if a streamline curves strongly at $y - 1 \ll 1$, the parallel component of gravity may increase rapidly with y, while for streamlines which remain nearly vertical over $y - 1 \ll 1$, gravity is roughly proportional to $y - 1$ and centrifugal force does not

affect motion along a streamline. However, if angular momentum is conserved along a streamline, then approximate balance of gravity and centrifugal force to $\sim O(y - 1)$ will hold in the range $1 < y \lesssim 2$, regardless of the trajectory. The *effective* gravity is relatively insensitive to trajectory, despite the fact that gravity and centrifugal force each depend on it rather strongly. At $y \gtrsim 2$, we expect all trajectories to be approximately radial, with $yR_0 \approx R \equiv$ spherical radius; hence $g(r)$ tends in this regime toward the total gravity. Specifically, we take

$$g(r) \equiv g_0(R_0)f_g(y) ,\qquad (3.6)$$

where, for a thin disk,

$$g_0(R_0) = \frac{GM}{R_0^2} , \quad f_g(y) = \frac{y - 1}{y^3} .\qquad (3.7)$$

The tendency of f_g to diminish as $y \to 1$ reflects the fact that the gravitational binding energy of material in a Keplerian disk is only half that of stationary material, and hence less work is required to unbind it. For flows in which gravity determines the mass flux (cf. § IIId), this results in larger outflow than would occur in a non-rotating flow with the same geometry.

Conservation of energy is most conveniently expressed in terms of an entropy equation,

$$\frac{3}{2} pv \frac{d}{dr} \ln\left(\frac{p}{\rho^{5/3}}\right) = n_e \Gamma(r, T) ,\qquad (3.8)$$

where T is the temperature, n_e is the electron density, and Γ is the heating rate per unit mass. Equation (3.8) is easily converted to an enthalpy equation through the use of equations (3.4) and (3.5). For optically thin flow, the spatial dependence of Γ may be specified in advance as a function of R, and approximated (for a given streamline) in terms of yR_0 if $|\partial \ln \Gamma/\partial \ln R| < O(1)$. In this paper, we consider only Compton heating, which typically dominates at T greater than a few times 10^6 K (KMT), so that

$$\Gamma(r, t) = \Gamma_0(R_0)f_\Gamma(y)(1 - T/T_{IC}) ,\qquad (3.9)$$

where T_{IC} is defined in equation (2.4). The form factor $f_\Gamma(y)$ is determined by the unknown trajectories of the streamlines. For an isotropic central source of radiation, we consider two extreme cases: Case 1 is vertically rising outflow, $f_\Gamma = [1 + (y - 1)^2]^{-1}$; case 2 is radial outflow, $f_\Gamma = y^{-2}$.

Finally, we have the boundary conditions appropriate to wind solutions,

$$v = T = 0 , \quad p = p_0 \quad \text{at} \quad y = 1 ,\qquad (3.10)$$

where $p_0(R_0)$ is the critical pressure discussed in § II. At $y \to \infty$ the pressure vanishes, and we shall seek solutions which pass through a critical point and become supersonic. As in standard accretion and wind problems, the latter condition is sufficient to determine a unique mass flux.

b) Dimensionless Equations

The flow equation can be made dimensionless by eliminating ρ through the equation of state $p = \rho k T/\mu$ and introducing the dimensionless variables

$$T^* = \frac{T}{T_{ch}} , \quad p^* = \frac{p}{p_0} , \quad \mathcal{M} = \frac{v}{c} ,\qquad (3.11)$$

where T_{ch} is defined in equation (2.9), $c = (kT/\mu)^{1/2}$ is the isothermal sound speed, and $\mathcal{M}$ is the isothermal Mach number. The dimensionless mass flux is

$$\dot{m}^* \equiv \frac{\dot{m}}{m_{ch}} \equiv \frac{\dot{m}}{p_0/c_{ch}} .\qquad (3.12)$$

The continuity equation (3.4) becomes

$$p^* = \dot{m}^* T^{*1/2}/\mathcal{M} y^{\langle\beta\rangle} .\qquad (3.13)$$

The equation of motion (3.5) may be written in two equivalent ways as

$$-\frac{d \ln p^*}{dy} = \frac{d \ln (1 + \mathcal{M}^2)}{dy} + \frac{\mathcal{M}^2}{1 + \mathcal{M}^2} \frac{\beta}{y}$$
$$+ \frac{f_g}{(1 + \mathcal{M}^2)\alpha^2 T^*}\qquad (3.14a)$$

or as

$$(\mathcal{M}^2 - 1)\frac{d \ln \mathcal{M}^2}{dy} + (\mathcal{M}^2 + 1)\frac{d \ln T^*}{dy} = \frac{2\beta}{y} - \frac{2f_g}{\alpha^2 T^*} .$$
$$(3.14b)$$

The entropy equation (3.8) is

$$\frac{d}{dy}\left(p^{*1/5}\mathcal{M} T^{*3/2} y^{\langle\beta\rangle}\right) = \left(\tfrac{2}{5}\right)f_\Gamma \, p^{*1/5} y^{\langle\beta\rangle}(1 - T^*/T_{IC}^*) ,$$
$$(3.15)$$

where we have used $n_e = \rho/\mu_e \approx \rho/2\mu$ to obtain the right hand side of (3.15). The dimensionless boundary conditions are $\mathcal{M} = T^* = 0$, $p^* = 1$ at $y = 1$.

c) Sonic Points

The momentum and entropy equations can be manipulated to give

$$(3\mathcal{M}^2 - 5)\frac{d \ln \mathcal{M}^2}{dy} = \frac{2\beta}{y}(5 + \mathcal{M}^2) - \frac{(\mathcal{M}^2 + 1)f_\Gamma}{\mathcal{M} T^{*3/2}}$$
$$\times \left(1 - \frac{T^*}{T_{IC}^*}\right) - \frac{8f_g}{\alpha^2 T^*} .\qquad (3.16)$$

The adiabatic sonic point ($\mathcal{M}^2 = 5/3$) is a critical point of this equation. Wind solutions, which make the transition from subsonic to supersonic flow, must pass through this point, yielding the auxiliary condition

$$\frac{5\beta_s}{y_s} = \left(\frac{3}{5}\right)^{1/2}\frac{f_{\Gamma_s}}{T_s^{*3/2}}\left(1 - \frac{T_s^*}{T_{IC}^*}\right) + \frac{3f_{gs}}{\alpha^2 T_s^*} ,\qquad (3.17)$$

where subscript s denotes evaluation at the adiabatic sonic point y_s. Note that gravity and heating contribute

to the auxiliary condition with terms of the same sign, implying that the flow must diverge ($\beta_s > 0$) in order for a sonic point to exist. This statement does not contradict the results of London and Flannery (1981), who found transonic solutions for plane-parallel flow, because they considered a gravitational field which changes sign (at a Lagrangian point) while we assume that f_g is positive everywhere.

In some cases the flow is nearly isothermal, and the condition that the solution pass through the isothermal sonic point (denoted y_1) gives the condition (from eq. [3.14b])

$$y_1 = \frac{1}{\beta_1 \alpha^2 T_1^*}\left(1 - \frac{1}{y_1}\right), \qquad (3.18)$$

provided $d \ln T^*/dy \ll \beta_1/y_1$. This is a critical point of the system of equations only if T^* is set constant.

d) Flows with Steady Heating

i) General Results

If $T \ll T_{\text{IC}}$, as in regions B and C of Figure 1, the heating rate Γ becomes insensitive to temperature and it is possible to obtain accurate approximate integrals for the entropy and momentum equations. In this case, the right-hand side of the entropy equation (3.15) then depends on hydrodynamic variables only through a factor $p^{*1/5}$. The weakness of this dependence results from the form of the heating function, as well as the proximity of the adiabatic index ($\gamma = 5/3$) to 2. If γ equaled 2, the $p^{*1/5}$ dependence would disappear and the analog of (3.15) would be exactly integrable. We can write the integral of (3.15) with steady heating in the form

$$\mathcal{M}T^{*3/2} = \frac{(2/5)\eta}{y^{\langle\beta\rangle}}\int_1^y f_\Gamma y^{\langle\beta\rangle}dy \qquad (3.19)$$

with

$$\eta \equiv \frac{\left(\int_1^y f_\Gamma p^{*1/5} y^{\langle\beta\rangle}dy\right)}{\left(p^{*1/5}\int_1^y f_\Gamma y^{\langle\beta\rangle}dy\right)}, \qquad (3.20)$$

where we have taken $\mathcal{M}T^{*3/2} = 0$ at $y = 1$, the disk surface. If p^* does not vary too strongly with y, η will remain close to unity. In any case, since p^* is a decreasing function of y, we have $\eta \geq 1$.

In order to evaluate the integral in equation (3.19), we make use of the fact that f_Γ is bounded from above by $[1 + (y - 1)^2]^{-1}$—the case of vertical outflow—and from below by y^{-2}—the case of spherical outflow. In either case, we approximate

$$\frac{1}{y^{\langle\beta\rangle}}\int_1^y f_\Gamma y^{\langle\beta\rangle}dy \approx \left(\frac{f_\Gamma}{y^{\langle\beta\rangle}}\right)^{1/2}(y - 1) \qquad (3.21)$$

with an accuracy of better than a factor 1.5 for $y \lesssim 20$ and $\langle\beta\rangle = $ const. between 0 and 2. For $y \gg 20$, the factor $y^{\langle\beta\rangle}$ on the right-hand side of equation (3.21) should be replaced by $y^{\min(2\beta, 2)}$ to obtain the correct asymptotic behavior.

At the sonic point, equation (3.19) becomes

$$\left(\frac{5}{3}\right)^{1/2}T_s^{*3/2} = \frac{2}{5}\eta_s\left[\frac{f_{\Gamma_s}}{y_s^{\langle\beta\rangle}}\right]^{1/2}(y_s - 1). \qquad (3.22)$$

When substituted into the critical point condition (3.17), this yields (recall $T \ll T_{\text{IC}}$)

$$\frac{\beta_s}{y_s} = \frac{1}{2}\frac{f_{\Gamma_s}^{1/2}y_s^{\langle\beta\rangle/2}}{\eta_s(y_s - 1)} + \left(\frac{3}{2\eta_s}\right)^{2/3}\frac{(y_s - 1)^{1/3}}{a^2 y_s^{3 - \langle\beta\rangle/3}f_{\Gamma_s}^{1/3}}. \qquad (3.23)$$

The two terms on the right-hand side represent the effects of Compton heating and gravity, respectively.

The equation of motion (3.14a) can now be integrated by using equations (3.13) and (3.19) to eliminate T^* in favor of p^* and y. The result is

$$p^* = \frac{[1 - (5\dot{m}^*/8\alpha^4)^{1/2}I_g]^2}{1 + \mathcal{M}^2}y^{-\beta\mathcal{M}^2/(1+\mathcal{M}^2)}, \qquad (3.24)$$

where

$$I_g = \int_1^y \frac{f_g}{\eta^{1/2}f_\Gamma^{1/4}}\frac{y^{\langle\beta[(\mathcal{M}^2-1)/(\mathcal{M}^2+1)]\rangle/4}}{(1 + \mathcal{M}^2)(y - 1)^{1/2}}dy \qquad (3.25)$$

and

$$\langle x\rangle \equiv \frac{1}{\ln y}\int_1^y x\frac{dy}{y}. \qquad (3.26)$$

Equations (3.13) and (3.22–3.24) allow us to determine y_s, T_s^*, p_s^*, and $\dot{m}^*$ for an assumed flow divergence, represented by β and f_Γ. A related problem of interest is that of spherical outflow with spatially uniform heating ($f_\Gamma = 1$), since the latter is formally identical to the suprathermal, Coulomb heated ("SCH") evaporation flow analyzed by Balbus and McKee (1982). In this case equation (3.19) can be integrated exactly, and our method (with $\eta \approx 1$) gives a value for $\dot{m}^*$ within 6% of their exact result.

We now obtain explicit solutions for the cases $\alpha \gg 1$ (extreme Region B) and $\alpha \ll 1$ (extreme Region C).

ii) Steadily Heated, Free Wind (Region B)

When $\alpha \gg 1$, gravitational effects on the flow are negligible. Anticipating that $y_s \lesssim 2$, we approximate the exponents of y_s as $\langle\beta\rangle = (\frac{1}{2})\beta_s$, $\langle\beta F\rangle = \langle\beta\rangle\langle F\rangle$, and $\langle F(\mathcal{M}^2)\rangle = F(\mathcal{M}^2/2)$ (the accuracy of the last approximation has been verified by Balbus and McKee 1982); we also set $\eta_s \approx 1$. The critical point condition (3.23) then becomes

$$2\beta_s(y_s - 1) = y_s^{1 + (\beta_s/4)}f_{\Gamma_s}^{1/2}. \qquad (3.27)$$

The pressure (eq. [3.24]) and temperature (eqs. [3.22] and [3.27]) at the sonic point reduce to

$$p_s^* = (\tfrac{3}{8})y_s^{-(5\beta_s/22)}$$
$$T_s^* = 0.29(y_s f_{\Gamma_s}/\beta_s)^{2/3}. \qquad (3.28)$$

Finally, the mass loss rate is determined by the equation of continuity to be

$$\dot{m}^* = 0.90(\beta_s/f_{\Gamma_s})^{1/3}y_s^{3\beta_s/11 - 1/3}. \qquad (3.29)$$

First assume that f_Γ has its maximum possible value, corresponding to vertical outflow. In fact, the flow has a finite divergence, and this divergence is necessary to give a sonic point. For $y_s = (1.7, 2, 2.5)$, equation (3.27) gives $\beta_s = (1.2, 0.8, 0.5)$ and equation (3.29) gives $\dot{m}^* = (1.1, 1.0, 0.9)$. Note that the uncertainty in the location of the sonic point does not lead to a significant uncertainty in the mass loss rate. We expect $\beta_s \gtrsim 0.8$ at $y_s \sim 2$ and conclude $\dot{m}^* \gtrsim 1.0$. At $y_s = 2$, the temperature is $T_s^* = 0.33$ and the pressure is $p_s^* = 0.33$.

Next consider the opposite limit in which f_Γ corresponds to spherical outflow. In this case, $y_s = (1.3, 1.7, 2)$ corresponds to $\beta_s = (1.9, 0.8, 0.55)$ and $\dot{m}^* = (1.4, 1.1, 1.0)$. Since the upper bound on β_s is 2, we conclude $\dot{m}^* \lesssim 1.4$. At $y_s = 1.3$, we find $T_s^* = 0.16$ and $p_s^* = 0.33$.

We conclude that, independent of the precise manner in which the flow diverges from the disk, the mass loss rate is

$$\dot{m}^* = 1.2 \pm 0.2 \quad (\text{Region } B) . \qquad (3.30)$$

The temperature at the sonic point is $0.16 \lesssim T_s^* \lesssim 0.33$ and the pressure is $p_s^* \approx 0.33$.

The qualitative nature of the flow in this case can now be described. The flow reaches a critical point at $4/3 < y_s < 2$. Because of the short range of the subsonic regime, the divergence of the flow does *not* strongly affect the variation of flow parameters [i.e., $y^{\langle\beta\rangle} \sim O(1)$], despite the fact that the presence of nonnegligible divergence is responsible for the existence of the sonic point. Since gravity is unimportant, the pressure is roughly uniform, and we have

$$1 \approx \dot{m}^* = \frac{\rho v}{p_0} c_{\text{ch}} \approx \frac{v c_{\text{ch}}}{c^2} \approx \frac{\mathcal{M}}{T^{*1/2}} \qquad (3.31)$$

while $\mathcal{M} T^{*3/2} \sim y - 1$ from the heating equation (3.19). Thus the flow is characterized by

$$v \propto T^* \sim (y - 1)^{1/2} , \quad \mathcal{M} \sim (y - 1)^{1/4} \qquad (3.32)$$

in the subsonic regime. In the supersonic regime, we have $y \gg 1$, $\beta \approx 2$, and the pressure declines:

$$p^* \sim \frac{1}{\mathcal{M}^2 y^2} \sim \frac{T^{*1/2}}{\mathcal{M} y^2} , \qquad (3.33)$$

while the declining heating rate ($\Gamma \propto y^{-2}$) is only partially able to compensate for adiabatic losses,

$$\mathcal{M} T^{*3/2} \sim 1/y . \qquad (3.34)$$

As a result, we obtain a wind solution with

$$v \sim \text{const.} , \quad T^* \propto y^{-1} , \quad \mathcal{M} \propto y^{1/2} , \quad p^* \propto y^{-3} , \qquad (3.35)$$

which we refer to as the constant velocity, non-isothermal flow pattern. Note that the temperature reaches a maximum $\sim T_{\text{ch}}$ near the sonic point.

iii) Gravity-inhibited Wind (Region C)

When $T_g \gg T_{\text{ch}}$ ($\alpha \ll 1$), gravitational effects significantly impede the wind. Bardeen and Berger (1978) have obtained a self-similar solution for this class of problems, and they find that for a central point mass

and a disk pressure proportional to y^{-2} the flow asymptotically approaches $\beta = 1.2$. As discussed at the outset of § III, our problem is not self-similar and we anticipate $\beta \to 2$, at least near the edge of the disk where the mass loss is greatest. Although the location of the sonic point is sensitive to the asymptotic value of β, the mass loss rate is not, so this uncertainty is not important.

Solution of equation (3.23) shows that the adiabatic sonic point occurs far from the disk when $\alpha \ll 1$:

$$y_s^{1 - \langle\beta\rangle/3} \approx \left(\frac{3}{2\eta_s}\right)^{2/3} \frac{1}{\alpha^2 \beta_s} \gg 1 , \qquad (3.36)$$

where we have neglected the first term on the right-hand side of (3.23). This is a good approximation for $\langle\beta\rangle < 2$, but for $\langle\beta\rangle = 2$, $y_s^{1/3}$ should be increased by a factor $4\eta_s/(4\eta_s - 1)$. The temperature at the sonic point is $T_s^* \sim y_s^{-\langle\beta\rangle/3} \ll 1$. Inserting expression (3.24) for p^* into equation (3.13) and solving, we obtain

$$\dot{m}^* = [0.79 I_{gs} \alpha^{-2} + 1.43 T_s^{*1/4} y_s^{-\langle\beta/(1 + \mathcal{M}^2)\rangle/2}]^{-2} , \qquad (3.37)$$

where I_{gs} is the integral I_g (eq. [3.25]) evaluated at y_s. For $\alpha \ll 1$, the second term is negligible and we find

$$\dot{m}^* = 1.6 \alpha^4 I_{gs}^{-2} . \qquad (3.38)$$

Since I_{gs} is dominated by the contribution from $y \sim O(1) \ll y_s$, we may approximate it by extending the upper limit of integration to infinity and by setting $1 + \mathcal{M}^2$ and η equal to 1; this yields

$$I_{gs} = \int_1^\infty (y - 1)^{1/2} y^{-3} (y^{\langle\beta\rangle} f_\Gamma)^{-1/4} dy . \qquad (3.39)$$

In the limiting case of spherical outflow, one has $\langle\beta\rangle = 2$ and $y^{\langle\beta\rangle} f_\Gamma = 1$, so that $I_{gs} = B(3/2, 3/2) = 0.39$, where $B(m, n)$ is the beta function. In the opposite limit of vertical flow, $\langle\beta\rangle = 0$ and numerical evaluation of the integral gives $I_{gs} = 0.58$. Adopting a value intermediate between these two cases, we set $I_{gs} = 0.5$ and obtain

$$\dot{m}^* = 6.4 \alpha^4 \ll 1 \quad (\text{Region } C) . \qquad (3.40)$$

This gravity-dominated flow is characterized by three regimes, two of them subsonic. In the first subsonic regime, $y \sim O(1)$ and I_g in (3.24) is sufficiently far from its asymptotic limit that the term in square brackets is $O(1)$. Thus the pressure is roughly uniform and the flow is characterized by the same *scaling* as (3.31) and (3.32). The *normalization*, however, is different, since $\dot{m}^*$ is smaller by a factor $\sim \alpha^4$. Instead of $T^* \sim \mathcal{M}^2 \sim (y - 1)^{1/2}$, we have

$$T^* \sim \alpha^{-2} (y - 1)^{1/2} , \quad \mathcal{M} \sim \alpha^3 (y - 1)^{1/4} . \qquad (3.41)$$

In the second subsonic regime, $1 \ll y < y_s$ and $\mathcal{M}^2 \ll 1$. Setting $\langle\beta\rangle = 2$ for simplicity gives the pressure declining as

$$p^* \sim \frac{\alpha^4 T^{*1/2}}{\mathcal{M} y^2} \gtrsim [I_{gs} - I_g]^2 \gtrsim y^{-3} \qquad (3.42)$$

from equations (3.24), (3.25), (3.28), and (3.39). Inserting

this pressure variation into equation (3.20) yields $\eta_s = 2.5$; then, since $y_s \propto \alpha^{-6}$ (eq. [3.36]), we obtain $p_s^* = (1.58\alpha)^{18}$. Equation (3.34) still holds, and as a result the wind pattern has the constant velocity, non-isothermal flow pattern

$$v \sim \text{const.}, \quad T^* \sim (\alpha^2 y)^{-1}, \quad \mathcal{M} \sim \alpha^3 y^{1/2}. \quad (3.43)$$

Except for scaling factors, (3.43) is identical to (3.35), the *supersonic* solution for the heating-dominated case. In fact, this scaling continues smoothly into the super-sonic regime of gravity-dominated flow, suggesting that there is nothing very special about the critical point. Instead of being fixed by the sonic point conditions, the mass flux is determined by the requirement that $1 - [(5/8)(\dot{m}^*/\alpha^4)]^{1/2} I_g$ nearly vanish in the limit $y \gg 1$. Conditions at the sonic point provide a negligible correction to this result, confirming the implausibility that such a distant constraint could control flow near the disk surface.

Finally, we note from (3.41) that the maximum temperature reached in the gravity-dominated case is $\sim T_g$, the gravitational escape temperature from the disk. The gas is able to reach a higher temperature than in the heating-dominated case (by a factor $\sim \alpha^{-2}$) because the slower outflow velocity affords a longer time for heating. At large y, the temperature is fixed by equality between heating and flow times, kT/Γ and R/v respectively. Since v levels off at roughly the escape speed from the disk and $\Gamma \propto R^{-2}$, the temperature is comparable with the local escape temperature at all radii.

e) Isothermal Flows

So far, we have examined flows subject to steady heating. These reach maximum temperatures $T_{max} \sim$ max $[T_{ch}, T_g]$ at a distance $\sim R_0$ from the base of the flow. Such flows, however, are inconsistent with the heating function (3.9) if $T_{max} > T_{IC}$, i.e., if

$$T_{IC}^* < 1 + \alpha^{-2}. \quad (3.44)$$

For the latter case, we expect the temperature to approach T_{IC} at $(y - 1) \ll 1$, and to remain nearly constant over some range of y. The nature of the flow depends upon $\alpha^2 T_{IC}^* = \xi$. If $\alpha^2 T_{IC}^* \gg 1$, then the gas temperature in the isothermal zone greatly exceeds the escape temperature and gravitational forces have a negligible effect. In the opposite limit ($\alpha^2 T_{IC}^* \ll 1$), a quasi-static corona is formed and the wind is weak.

i) Isothermal Free Wind (Region A)

Region A of Figure 1 is characterized by strong heating ($T_{ch} > T_{IC}$ or $T_{IC}^* < 1$) and weak gravitational forces ($T_{IC} > T_g$ or $\xi = \alpha^2 T_{IC}^* \gg 1$). It occurs in an annulus of the disk $R_{iso} > R_0 > R_{IC}$ provided $L > L_{cr}$ (see § II). Reference to the momentum equation (3.14b) shows that the isothermal sonic point occurs close to the surface of the disk, either near the point at which T approaches T_{IC} so that $\beta \approx d \ln T^*/dy \ll 1$, or at the point y_1 in equation (3.18) where $\beta \approx (y_1 - 1)/\alpha^2 T_{IC}^* \ll 1$. (Note that for spherical outflow, with $\beta = 2$, the

isothermal sonic point must occur in the heating zone; cf. London and Flannery 1981.) For one-dimensional flow, $p + \rho v^2 = \text{const.}$ so that $p_1 = (\frac{1}{2})p_0$ and

$$\dot{m}^* = p_1^* y_1^{\langle \beta \rangle} T_1^{*-1/2} = \frac{1}{2T_{IC}^{*1/2}} \quad \text{(Region A)} \quad (3.45)$$

since $y_1 \approx 1$ and $T_1^* \approx T_{IC}^*$.

The critical point in the outflow (the adiabatic sonic point) occurs significantly farther from the disk surface. Neglecting the small gravitational term, we can integrate the momentum equation and find (cf. Balbus and McKee 1982)

$$\frac{T^*}{T_{IC}} = \frac{4\mathcal{M}^2}{(1 + \mathcal{M}^2)^2} y^{\langle \beta/(1 + \mathcal{M}^2)\rangle}, \quad (3.46)$$

where we have used the result (3.45) for $\dot{m}^*$. Hence $T \to T_{IC}$ as $\mathcal{M} \to 1$, and $\mathcal{M}$ can reach $(5/3)^{1/2}$ only when y and β are large enough.

In the supersonic regime ($y \gg y_s$) we set $\beta \approx 2$ and find

$$\mathcal{M}^2 \approx 4 \ln y, \quad p^* \approx [y^2(1 + \mathcal{M}^2)]^{-1}. \quad (3.47)$$

For the isothermal approximation to be self-consistent we require

$$T_{IC}^{*3/2} \ll \frac{2}{5} \eta \frac{\int_1^y f_\Gamma y^{\langle \beta \rangle} dy}{y^{\langle \beta \rangle}} \approx \frac{2}{5} \frac{y - 1}{y^2} \quad (3.48)$$

from equations (3.19) and (3.21). This condition breaks down at

$$y_i \sim 0.2(\ln y_i)^{-1} T_{IC}^{*-3/2} \gtrsim 2. \quad (3.49)$$

For $y > y_i$, the heating can no longer keep up with adiabatic cooling and the flow becomes non-isothermal. The flow then follows the constant velocity, non-isothermal pattern (eq. [3.35]), but with a different normalization.

ii) Corona with Weak Isothermal Wind (Region E)

Deep in Region E of Figure 1, the heating is strong ($T_{IC}^* \ll 1$, $L \gg L_{cr}$) as in the case above, but here gravitational forces are strong as well ($T_g \gg T_{IC}$, or $\xi = \alpha^2 T_{IC}^* \ll 1$). The isothermal sonic point (eq. [3.18]) occurs far from the disk surface,

$$y_1 = \frac{1}{\beta \alpha^2 T_{IC}^*} = \frac{1}{\beta \xi} \gg 1, \quad (3.50)$$

i.e., at $r = R_{IC}/\beta$, where T_{IC} is about equal to the local escape temperature T_g/y. Since $y_1 \gg 1$, we have assumed that β is constant and have set $\beta_1 = \beta$. The gas is nearly isothermal, so the pressure can be found from equation (3.14a) to be

$$p^* = (1 + \mathcal{M}^2)^{-1} \exp[-(1 - y^{-1})^2/2\xi] \quad (3.51)$$

which for $y \ll y_1$ is just an isothermal atmosphere. The mass loss rate is then

$$\dot{m}^* = \frac{1}{2T_{IC}^{*1/2}} \left(\frac{e}{\beta \xi}\right)^\beta \exp(-0.5\xi^{-1}) \quad (3.52a)$$

$$\to 0.9(\xi^2 T_{IC}^{*1/2})^{-1} \exp(-0.5\xi^{-1}) \quad \text{(Region E)}, \quad (3.52b)$$

where the second expression is for $\beta = 2$. Flow from the inner radii of the disk will be collimated by the flow from the outer parts of the disk, so that in the interior we expect β to be closer to 1.2, the value in Bardeen and Berger's similarity solution, than to 2. However, if the disk terminates at $R_d < R_{IC}$, the flow from the outer parts of the disk, which dominates the mass loss, will have $\beta \approx 2$. In this case the corona fills the volume inside R_{IC}, the area of the sonic surface is of order $R_{IC}^2 = R^2/\xi^2$, and equation (3.52b) shows that the mass loss rate is larger by a factor ξ^{-2} over what one might naively expect. Note that equation (3.52) is valid only for $\xi \ll 1$. In fact, we expect that $\dot{m}^*$ in Region E should be less than the value given by (3.45) for Region A, which implies that (3.52b) is valid for $\xi < 0.1$.

The condition for the flow to be isothermal out to the critical point may be inferred from the critical point condition (3.17),

$$y_s = 0.6 y_1 + \frac{1}{12.9 T_{IC}^*} \left(\frac{T_{IC} - T}{T} \right) . \qquad (3.53)$$

The requirements that the adiabatic sonic point at y_s occur outside the isothermal one at y_1 and that $(T_{IC} - T)/T$ be small imply

$$\alpha^2 T_{IC}^{*-1/2} \gg 1 , \quad \text{or} \quad L \gg L_{cr} . \qquad (3.54)$$

In the supersonic isothermal regime the flow parameters scale as in equation (3.47); once the flow becomes non-isothermal, the flow follows the scaling in (3.35).

iii) Corona with Weak Non-isothermal Wind (Region D)

In Region D, the heating is weak ($\alpha^2 T_{IC}^{*-1/2} < 1$, $L < L_{cr}$) and the gravity strong ($T_g > T_{ch}$ or $\alpha < 1$), so that the resulting wind is extremely weak. We therefore content ourselves with an approximate analysis. As in Region E, the sonic point occurs at large y; but as in Region C, the heating is inadequate to maintain $T = T_{IC}$ out to the sonic point. To determine where the isothermal approximation breaks down, we use the energy equation, which may be derived from the momentum and entropy equations. For $\mathcal{M} \ll 1$ and $y \gg 1$, we have

$$\frac{dT^*}{dy} = -\frac{2}{5\alpha^2 y^2} + \frac{1}{5\mathcal{M} T^{*1/2} y^2} \frac{T_{IC} - T}{T_{IC}} ; \qquad (3.55)$$

hence the temperature begins to drop below T_{IC} at $\mathcal{M} = \mathcal{M}_i \equiv (\frac{1}{2})\alpha^2 T_{IC}^{*-1/2} = L/2L_{cr} \ll 1$. The flow then enters the constant velocity, non-isothermal pattern, just as in Region C. In this case $\mathcal{M} T^{*1/2}$ is constant so that equation (3.55) can be integrated. One finds that $T^* y$ is a constant somewhat smaller than $0.4\alpha^{-2}$. Evaluating the mass loss rate by applying the continuity equation at y_i, the point at which $\mathcal{M} = \mathcal{M}_i$, we find that $\dot{m}^*$ is smaller than that in Region E by about a factor $\mathcal{M}_i$:

$$\dot{m}^*(\text{Region D}) \approx \frac{L}{L_{cr}} \dot{m}^*(\text{Region E}) . \qquad (3.56)$$

The constant velocity, non-isothermal flow pattern can be self-consistently extended out to the adiabatic sonic point only if $\beta > 1.5$; then one finds $r_s/R_{IC} \sim O(L_{cr}/L)^2$ and $T_s^* \sim O(\alpha^4) \ll 1$.

f) Summary

For $\xi = R_0/R_{IC} > 1$ there is a wind with a mass loss rate

$$\dot{m}^* = \frac{1}{2} \left(\frac{L}{L_{cr}} \right)^{1/3} \xi^{-1/3} \quad \text{(Region A)}$$

$$= 1.2 \qquad \text{(Region B)} \qquad (3.57)$$

$$= 6.4 \left(\frac{L}{L_{cr}} \right)^{4/3} \xi^{2/3} \quad \text{(Region C)}$$

in Regions A–C, respectively. For $\xi < 1$ (Regions D–E) a quasi-static corona forms and the mass loss rate is exponentially small; for $\xi \lesssim 0.1$, we estimate

$$\dot{m}^* \approx \frac{(L/L_{cr})^{4/3}}{1 + (L/L_{cr})} \xi^{-7/3} \exp(-0.5/\xi) . \qquad (3.58)$$

Here we have set $\beta = 2$, which is appropriate for the outer part of the disk. Curves corresponding to (3.57) and (3.58) are displayed in Figure 2.

The physical mass loss rate per unit area is $\dot{m} = \dot{m}^* \dot{m}_{ch} = \dot{m}^* p_0/c_{ch}$, where we recall that p_0 is the gas pressure at the base of the flow and $c_{ch} = (k T_{ch}/\mu)^{1/2}$ can be found from equation (2.9). If the incident X-rays are not attenuated while passing through the flow, then $p_0 \propto L/4\pi R_0^2, c_{ch} \propto R^{-1/3}$, and $\dot{m}_{ch} \propto \xi^{-5/3}$. If the X-rays are attenuated, then, as we pointed out in § II and
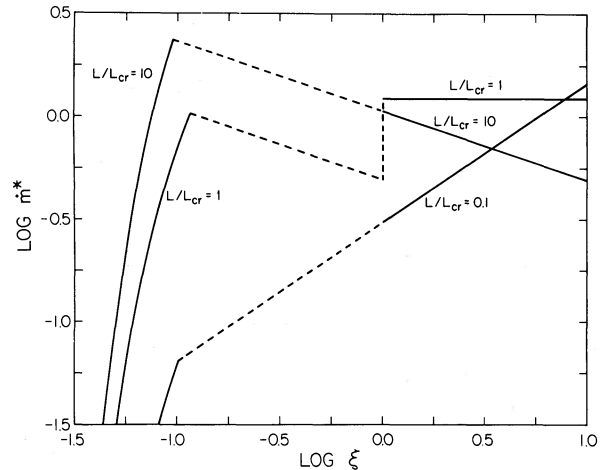

FIG. 2.—The normalized mass loss rate per unit area $\dot{m}^*$ (eqs. [3.12] and [3.57]) is plotted as a function of the normalized radius R/R_{IC}, with L/L_{cr} as parameter. The mass loss rate in the outer corona ($0.1 < \xi < 1$) is uncertain and is indicated by dashed lines; we have chosen to extrapolate the results from the wind region (eq. [3.57]) since this generally gives a lower mass loss than extrapolating from the inner corona ($\xi < 0.1$, eq. [3.58]). For $L/L_{cr} = 1$, we have extrapolated from Region A rather than from Region C since the result for the latter is valid only for $\alpha \ll 1$; the discontinuity at $\xi = 1$ indicates the magnitude of the error to be expected when the result for a given region is used at the boundary of that region.

demonstrate in Paper II, neither the form for $\dot{m}^*$ (given L_{cr} and ξ) nor the value of c_{ch} is altered; p_0 is reduced, but except perhaps in the inner corona, where $\dot{m}$ is already exponentially small, p_0 remains strictly proportional to J_0, the mean radiation intensity at the base of the flow. (In the inner regions of the corona, cooling by soft radiation emitted locally within the disk may reduce p_0 below the value that one would estimate by simply considering the transfer of X-rays to the base of the hot gas—see Paper II.) We can therefore characterize the effects of scattering in the corona and wind through a single "attenuation factor"

$$f_{\Gamma_0} \equiv f = \frac{4\pi J_0}{L/4\pi R_0^2} < 1 \qquad (3.59)$$

which multiplies the mass fluxes given above. In Paper II we estimate f in different regions of the disk, and find that it generally exceeds 0.1 in the wind zone. In terms of f, the pressure p_0 is

$$p_0 = \frac{Lf}{4\pi R_0^2 \, \Xi_0' \, c}, \qquad (3.60)$$

where Ξ_0' is evaluated at the base of the flow. In the wind $\Xi_0' = \Xi_{c,max}'$, whereas in the corona a range of values above $\Xi_{h,min}'$ are possible (Paper II).

IV. DYNAMICAL IMPLICATIONS FOR ASTROPHYSICAL ACCRETION DISKS

a) Mass Loss and Accretion Instability

If the disk extends out to a radius R_d, the total mass loss rate due to the wind on both sides of the disk is

$$\dot{M}_w = 4\pi \int_0^{R_d} \dot{m}(R_0) R_0 \, dR_0 . \qquad (4.1)$$

The characteristic mass loss rate from the disk is

$$\dot{M}_{ch} = 4\pi R_{IC}^2 \, \dot{m}_{ch}(\xi = 1)$$

$$= \frac{fL}{cc_{IC} \Xi_0'} \left(\frac{L_{cr}}{L}\right)^{1/3} \qquad (4.2)$$

$$= 4.5 \times 10^{-7} \frac{fL_{38}}{\Xi_0' \, T_{IC8}^{1/2}} \left(\frac{L_{cr}}{L}\right)^{1/3} M_\odot \, yr^{-1} .$$

In evaluating $\dot{M}_{ch}$, we used equation (3.60) and took the attenuation factor f to be constant in the part of the disk from which the wind arises. In terms of $\dot{M}_{ch}$, the total mass loss rate is

$$\dot{M}_w = \dot{M}_{ch} Q_m(\xi_d) , \qquad (4.3)$$

where

$$Q_m(\xi_d) = \int_0^{\xi_d} d\xi \xi^{-2/3} \dot{m}^* . \qquad (4.4)$$

Unfortunately, the analysis of § III is quite approximate for $\xi \sim 1$, and our estimate of $Q_m(\xi_d)$ must be correspondingly crude for $\xi_d \lesssim 1$. Recall that equation (3.58) for $\dot{m}^*$ in Regions D and E applies only for $\xi \lesssim 0.1$. Since this expression reaches a maximum in the

range $0.1 < \xi < 1$ which is unphysical, we adopt the expedient of extending the expressions for Regions A and C into Regions E and D, respectively; e.g., for $0.1 < \xi < 1$ and $L_{cr} < L < L_E$, which we write as $E(\xi > 0.1)$, we adopt $\dot{m}^* = 0.5(L/L_{cr})^{1/3} \xi^{-1/3}$ (see Fig. 2). Evaluation of the integral in (4.4) then leads to the approximate results (see Fig. 3)

$$Q_m(\xi_d) = \frac{1}{2}\left(\frac{L}{L_{cr}}\right)^{1/3} \ln(12.5\xi_d) \quad [A + E \, (\xi > 0.1)]$$

$$= 3.6(\xi_d^{1/3} - \tfrac{2}{3}) \qquad [B]$$

$$= 6.4\left(\frac{L}{L_{cr}}\right)^{4/3}(\xi_d - 0.08) \quad [C + D \, (\xi > 0.1)]$$

$$= \frac{1.8(L/L_{cr})^{4/3}}{1 + L/L_{cr}} \xi_d^{-1} e^{-\xi_d/2} \quad [D, E \, (\xi < 0.1)] .$$

$$(4.5)$$

These expressions have been adjusted so that they are continuous at $\xi = 0.1$. At the boundary between Regions A and B ($\xi = L/L_{cr} \geq 1$), Q_m is continuous to within about 5%. The continuity between Regions B and C and between E ($\xi > 0.1$) and D ($\xi > 0.1$) is much worse because the expression for $\dot{m}^*$ in Region C is valid only for $\alpha \ll 1$.

For a given value of L_E the largest mass loss rates occur for $L \sim L_E$ in Regions A and B. Note that our result for $\dot{M}_w$ is of the same order as that expected for a strong radiation-pressure driven wind, $\dot{M} \sim L/cv_{max}$ (Castor, Abbott, and Klein 1975), even though in our case the mass loss is due to radiative heating rather than radiation pressure. Correspondingly, one can show that the energy flux in the wind $(\frac{1}{2})\dot{M}_w v_{wind}^2$ is small compared to L: the decrease in v_{wind}^2 as R_0 increases outweighs the increase in $\dot{M}_w$ in Region B.

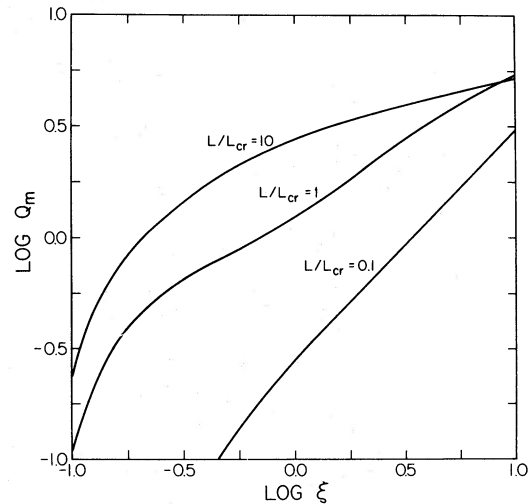Comparison of the mass loss from the disk with $\dot{M}_a$, the rate at which mass is accreted by the central object,

Fig. 3.—The integrated wind mass loss, normalized to $\dot{M}_{ch}$, is plotted as a function of the outer radius of the disk, normalized to R_{IC}, with L/L_{cr} as parameter (see eqs. [4.2]–[4.5]).

reveals an important result. In terms of the radiative efficiency

$$\epsilon = L/\dot{M}_a c^2 \qquad (4.6)$$

which is typically of order 0.1, the characteristic mass loss rate (eq. 4.2) is

$$\frac{\dot{M}_{ch}}{\dot{M}_a} = \frac{25.8\epsilon_{-1}f}{\Xi_0' T_{IC8}^{1/2}}\left(\frac{L_{cr}}{L}\right)^{1/3} . \qquad (4.7a)$$

In Regions A, B, and E ($\xi > 0.1$), where $L \gtrsim L_{cr}$ or ξ_d is large, the mass loss rate in the wind $\dot{M}_w = \dot{M}_{ch}Q_m(\xi_d)$ typically exceeds $\dot{M}_{ch}$. Hence, unless the flow is inefficient ($\epsilon_{-1} \ll 1$), or the outer disk is shadowed ($f \ll 1$) or severely truncated ($\xi_d \ll 1$), the mass loss in the wind exceeds the accretion rate by the central object in this case. In Regions C and D ($\xi > 0.1$), where $L < L_{cr}$, the factor Q_m may be small; the ratio $\dot{M}_w/\dot{M}_a$ in this case is

$$\frac{\dot{M}_w}{\dot{M}_a} = \frac{165\epsilon_{-1}f}{\Xi_0' T_{IC8}^{1/2}}\left(\frac{L}{L_{cr}}\right)(\xi_d - 0.08) , \quad C + D \ (\xi > 0.1) \qquad (4.7b)$$

from equations (2.12b), (4.5), and (4.7a). For $L \ll L_{cr}$, the attenuation factor f approaches unity (Paper II); hence accreting neutron stars or black holes with $\epsilon_{-1} \sim 1$ and with low luminosity can easily have $\dot{M}_w/\dot{M}_a > 1$. For accretion onto white dwarfs, the efficiency is so low ($\epsilon_{-1} \sim 10^{-2}$) that this condition is difficult to attain.

Disks with $\dot{M}_w \gg \dot{M}_a$ are likely to be unstable since small fluctuations in L can lead to small fluctuations in $\dot{M}_w$ which then get magnified into a large fluctuation in $\dot{M}_a$. Because it takes the accreting gas a finite time Δt to go from the wind region to the central object, this instability is likely to be manifested as overstability. A similar situation has been discussed by Arons (1973) in connection with self-excited flow in binary X-ray sources in which the X-ray source drives a wind from the companion star instead of from the disk.

We demonstrate the existence of the instability through a simple mathematical model. Suppose $\dot{M}_{in}$ is the rate at which mass is injected into the disk, and that the mass accreted at time t is simply the mass which is not blown away in a wind at $t - \Delta t$:

$$\dot{M}_a(t) = \dot{M}_{in}(t - \Delta t) - \dot{M}_w(t - \Delta t) . \qquad (4.8)$$

This neglects the radial variation of $\dot{M}_w$ and the time variation of the disk mass; it is thus equivalent to having the wind arise from a ring of fixed mass. We also assume that the mass loss in the wind is a fixed constant times the luminosity and hence the accretion rate:

$$\dot{M}_w(t) = C\dot{M}_a(t) . \qquad (4.9)$$

If $\dot{M}_{in}(t) = \dot{M}_0$, a constant, for $t < 0$ and $\dot{M}_{in}(t) = \dot{M}_0 + A \sin \omega t$ for $t > 0$, then equations (4.8) and (4.9) can be solved by Laplace transforms:

$$\dot{M}_a(t) = \dot{M}_0(1 + C)^{-1} + A\sum_{n=1}^{m}(-C)^{n-1}\sin \omega(t - n\Delta t) , \qquad (4.10)$$

where m is the greatest integer in $t/\Delta t$. If the wind mass loss is less than the accretion rate ($C < 1$), then the series converges and the flow is stable; but in the opposite case ($C > 1$) the series diverges in an alternating fashion and the flow is unsteady. The critical value of C required for the onset of instability depends on the assumptions in the model; for example, allowing the disk mass to vary leads to $C \gtrsim 2$ for instability. In this simple model the accretion eventually will become intermittent, alternating between ON states of normal luminosity and OFF states of negligible luminosity. The characteristic time scale for the ON and OFF states is given by the inflow time from the radius R_0 of the ring; for a standard α-model disk (Shakura and Sunyaev 1973), this is

$$\Delta t = \alpha_d^{-1}(h_d'/R_0)^{-2}t_g(R_0)$$
$$= 85\alpha_d^{-1}(h_d'/R_0)^{-2}(M/M_\odot)(\xi/T_{IC8})^{3/2} \text{ s} , \qquad (4.11)$$

where t_g is the free-fall time and h_d' is the scale height of the disk. (Note that h_d' may differ from the height h_d of the disk surface above the midplane—see below.)

In a more realistic disk, the wind arises over a range of radii, $\xi \gtrsim 0.1$. Let Σ be the surface density of the disk and $\dot{\Sigma} = 2\dot{m}(\xi)$ be the rate at which Σ decreases due to the wind. Then the characteristic time for the wind to destroy the disk at ξ is $t_w = \Sigma/\dot{\Sigma}$. Gas is resupplied at ξ by inflow in a time $\Delta t = 2\pi R^2\Sigma/\dot{M}(\xi)$, where $\dot{M}(\xi)$ is the mass inflow rate in the disk at ξ. With the aid of equation (4.2), we find that the ratio of these times is

$$\frac{\Delta t}{t_w} = \frac{\dot{M}_{ch}}{\dot{M}(\xi)}\dot{m}^*\xi^{1/3} . \qquad (4.12)$$

For $\xi \lesssim 0.1$, the wind mass loss is exponentially small ($\dot{m}^* \to 0$) and $\dot{M}(\xi) \approx \dot{M}_a$; then $\Delta t/t_w \ll 1$ so that the surface density is controlled by inflow rather than by mass loss. However, if $\dot{M}_{ch}/\dot{M}_a \gtrsim 1$, then at some radius $\xi_w > 0.1$ the integrated wind mass loss $\dot{M}_w$ ($\xi < \xi_w$) equals the accretion rate $\dot{M}_a$. For $\xi > \xi_w$, the surface density is controlled by the wind mass loss (which implies $\dot{M}(\xi) \sim \dot{M}_w(<\xi)$, so that $\Delta t \sim t_w$ from eq. [4.12]), and the instability can operate. Since $\Delta t(\xi) \propto \xi^{3/2}(h_d'/R)^{-2}$ increases with radius, so does $t_w(\xi)$: when the disk has been burned away at ξ_w, it will still be intact at $\xi \gg \xi_w$. Hence we expect the dominant time scale for the instability to be of order $\Delta t(\xi_w) \sim t_w(\xi_w)$. The outer part of the disk ($\xi \gg \xi_w$) is unaffected by these fluctuations, but it may well be unstable on a longer time scale. For $\dot{M}_{ch}/\dot{M}_a \gg 1$, we estimate $\xi_w \sim 0.2$ from equation (4.5) so that

$$\Delta t(\text{instability}) \sim 3 \times 10^3 \frac{(M/M_\odot)}{\alpha_d T_{IC8}^{3/2}}\left(\frac{R}{20h_d'}\right)^2 \text{ s} . \qquad (4.13)$$

For stellar X-ray sources this is of order an hour, whereas for disks in active galactic nuclei it is of order 10^4 yr. Because of this competition between inflow and mass loss, the instability may saturate at a finite amplitude rather than going to the limit in which the luminosity alternates between on and completely off. Radiative transfer effects (Paper II) can considerably complicate

this simple picture, though: if the attenuation factor f is small at $\xi \sim 0.2$ and increases outward, then ξ_w may be determined by the variation in f. In principle, the height of the disk could be altered by the mass loss, which would greatly complicate the instability since f depends on the shape of the disk. In Appendix B we discuss the vertical structure of the disk and show that this is not a problem.

A possible example of this instability is provided by 4U 1626−67, an X-ray pulsar which exhibits flares which recur approximately every $1–3 \times 10^3$ s (Li *et al.* 1980; Middleditch *et al.* 1981). Its hard spectrum corresponds to $T_{IC} \approx 10^8$ K. Middleditch *et al.* (1981) have determined its binary period to be 2500 s and have inferred $h_d/R \lesssim 0.05$. If h'_d/R is close to this maximum value and if $\alpha_d \sim 1$, then equation (4.13) shows that the predicted instability time scale is close to the observed one. Such flaring has not been reported in other binary X-ray sources, however, so this argument is far from conclusive. The most likely explanation for the absence of flaring is that the attenuation factor f is too small for the instability to operate. As shown in Paper II, such small values of f are easily possible, but the theory is not sufficiently exact to explain why a sufficiently large f is found only in 4U 1626−67. In the case of Her X-1, McCray *et al.* (1982) account for the observed soft X-ray flux by reprocessing of the hard X-rays at the "inner" edge of the accretion disk, which is assumed to be thickened by interaction with the magnetosphere; such a configuration would lead to small f and eliminate the instability. If this model is correct, then soft X-ray excesses should be anticorrelated with flaring. A search for flaring behavior in other sources would be worthwhile.

The unsteady disk accretion we find for high efficiencies and luminosities is the two-dimensional analog of the X-ray preheating instability in spherical accretion (Ostriker *et al.* 1976; Cowie, Ostriker and Stark 1978; Krolik and London 1983). In our case, the existence of the instability depends on the shape of the disk; if the disk does not flare, the attenuation factor f will be small and the instability will not occur at all. There are several effects which can thicken the outer disk and thus enhance the instability: The disk may be "twisted" so that the planes of the inner and outer disks are not coincident (Bardeen and Petterson 1975), as has been suggested for Her X-1 (Roberts 1974; Petterson 1977). Second, if the disk in a binary system is large enough that the trajectories of the orbiting particles intersect (Paczyński 1977), then the outer disk will be heated and will thicken. Finally, it must be remembered that the effective thickness of the disk is not the scale height, but rather the point at which the pressure has dropped sufficiently far that $\Xi = \Xi_{c,max}$, which could be several scale heights above the plane (cf. Appendix B).

b) Angular Momentum Loss and Disk Truncation

The fundamental problem in the theory of accretion disks is the mechanism of angular momentum transport. This problem divides into two parts (Shu and Lubow

1981): transport within the disk and removal of angular momentum from the disk as a whole. In binary systems, it is thought that tidal interactions remove angular momentum by transferring it from the disk to the orbital motion of the stars. For accretion disks in active galactic nuclei, Gunn (1979) has suggested that angular momentum may be removed by viscous interaction with a nonrotating, hot ambient gas, whereas Blandford and Payne (1982) have suggested magnetic braking. Winds from accretion disks remove angular momentum as well as mass and thus provide yet another mechanism for angular momentum removal. Winds may act in concert with tidal interaction or magnetic braking, and their effectiveness should be inferable from observation. We shall calculate the angular momentum loss due to a Compton heated wind, although the mechanism is independent of the origin of the wind.

Let $\tilde{j}$ be the angular momentum per unit mass. For gas in a Keplerian orbit we have

$$\tilde{j} = R_{IC} c_{IC} \xi^{1/2} . \tag{4.14}$$

The angular momentum carried off by the wind is then

$$4\pi \int_0^{R_d} \dot{m}(R_0)\tilde{j}(R_0)R_0 \, dR_0 = \dot{M}_{ch} R_{IC} c_{IC} Q_j(\xi_d) , \tag{4.15}$$

where

$$Q_j(\xi_d) = \int_0^{\xi_d} d\xi \, \xi^{-1/6} \dot{m}^* . \tag{4.16}$$

The average value of $\tilde{j}$ in the wind is $R_{IC} c_{IC} \langle \xi^{1/2} \rangle$, where

$$\langle \xi^{1/2} \rangle = Q_j/Q_m \le \xi_d^{1/2} . \tag{4.17}$$

Approximate evaluation of Q_j leads to

$$\frac{Q_j(\xi_d)}{Q_m(\xi_d)} = \xi_d^{1/2}(1 - 0.28\xi_d^{-1/2})/\ln (12.5\xi_d)^{1/2}$$
$$[A + E \, (\xi > 0.1)]$$
$$= 0.4\xi_d^{1/2} \left[\frac{1 - 0.5(L/L_{cr})^{0.7}\xi_d^{-5/6}}{1 - 0.67\xi_d^{-1/3}} \right] \quad [B]$$
$$= 0.67\xi_d^{1/2}(1 - 0.022/\xi_d^{3/2})/(1 - 0.08/\xi_d)$$
$$[C + D \, (\xi > 0.1)]$$
$$= \xi_d^{1/2} \quad [D, E \, (\xi < 0.1)] . \tag{4.18}$$

The comments on the approximations below equation (4.5) apply here also.

We now focus on the case of semidetached binaries, in which accretion is due to Roche lobe overflow. As we shall see, a sufficiently strong wind can truncate the disk at a radius smaller than it would otherwise have. The gas injected into the accretion disk has an angular momentum corresponding to a circular orbit about the accreting star at a radius R_{in}. Flannery's (1975) calculation of R_{in} can be fitted to within a few percent by

$$\frac{R_{in}}{a} = \frac{0.1\tilde{\mu}}{1 - 0.8\tilde{\mu}^{4.2}} + 0.036 , \tag{4.19}$$

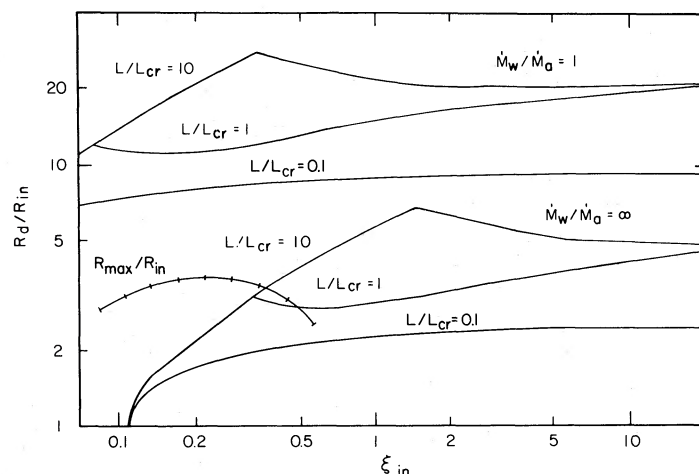where $0.05 \le \tilde{\mu} = M_x/M_{tot} \le 0.95$ is the fraction of the

FIG. 4.—Disk truncation by a Compton-heated wind: R_d/R_{in} is plotted as a function of ξ_{in}. The lower curves give the minimum possible disk size: for $\dot{M}_w/\dot{M}_a \to \infty$, where $\dot{M}_w$ is the mass loss in the wind, the angular momentum per gram carried off in the wind is equal to the injected angular momentum per gram. Note that R_d/R_{in} is independent of L/L_{cr} in Regions A + E ($\xi > 0.1$). The upper curves give R_d/R_{in} for $\dot{M}_w = \dot{M}_a$. Curves for $\dot{M}_w = \dot{M}_a/a$ can be obtained by displacing a point on one of the curves for $\dot{M}_w/\dot{M}_a = \infty$ to the left by a factor $(1 + a)^2$ and then up by the same factor. The normalized maximum disk radius R_{max}/R_{in} given by the Paczyński-Smak tidal truncation theory (eq. [4.20]) is shown for a range of values of the mass ratio $\tilde{\mu}$; it is independent of ξ_{in}. Tick marks indicate values of $\tilde{\mu}$ from 0.1 at the left to 0.9 on the right. The disk is truncated by a wind at R_d rather than at R_{max} only for small ξ_{in} and large $\dot{M}_w/\dot{M}_a$.

mass in the two stars which is in the X-ray source; a is the separation between the two stars, which are assumed to be in synchronous rotation. Angular momentum transport within the disk will cause the disk to spread outside R_{in}. Smak (1976) and Paczyński (1977) showed that, at a radius somewhat greater than R_{in}, particle orbits begin to intersect, and they suggested that this is likely to be the termination point of the disk. When the orbits begin to intersect, they are elliptical, and they have a maximum distance R_{max} from the accreting star of about 2–3.5 times R_{in} (for $0.05 \leq \tilde{\mu} \leq 0.95$). More precisely, in this mass range

$$R_{max}/R_{in} \approx 2.4 + 3.5\tilde{\mu} - 4.4\tilde{\mu}^3 \qquad (4.20)$$

to within about 5%. For $\tilde{\mu} \gtrsim 0.8$, orbits at R_{max} are unstable and the disk may be up to 20% smaller than this (Paczyński 1977). When the orbits intersect, one expects that turbulence will be generated which will facilitate the removal of angular momentum by tidal interaction. Observations of cataclysmic variables quoted by Paczyński (1977) support the idea that the disks are indeed somewhat smaller than R_{max}. In X-ray binaries, the heating associated with orbital intersection should thicken the disk and thus enhance the mass loss due to the Compton-heated wind.

To analyze the disk truncation due to a Compton-heated wind, we assume that the accretion is steady, that $f = $ const., and that the wind is the dominant mechanism for removing angular momentum from the disk. Balancing the angular momentum $\dot{M}_w R_{IC} c_{IC} \langle \xi^{1/2} \rangle$ carried away by the wind (see [eq. 4.17]) with the injected angular momentum $\dot{M}_{in} R_{IC} c_{IC} \xi_{in}^{1/2}$, we find

$$(\dot{M}_w + \dot{M}_a)\xi_{in}^{1/2} = \dot{M}_w Q_j/Q_m , \qquad (4.21)$$

where we used the relation $\dot{M}_{in} = \dot{M}_a + \dot{M}_w$. The solution of this equation gives R_d/R_{in}, as shown in Figure 4; R_{max}/R_{in} is plotted there also for comparison. In order for a Compton-heated wind to be more effective at truncating the disk than the Paczyński-Smak mechanism $(R_d < R_{max})$, large values of $\dot{M}_w/\dot{M}_a$ are required; for $L/L_{cr} > 1$, small values of ξ_{in} are needed as well. Since we have argued that accretion flows with $\dot{M}_w > \dot{M}_a$ are unstable, we conclude that disks truncated by a Compton-heated wind should exhibit unstable accretion. The converse will often be true if ξ_{in} is small; thus the disk in 4U 1626−67, which has $\xi_{in} \approx 0.4$ based on parameters from Middleditch et al. (1981), should be truncated by a Compton-heated wind. Other examples will be discussed in Paper II.

Our discussion up to this point has concentrated on X-ray binaries. In principle, winds could occur in cataclysmic variables, but the lower coronal temperatures imply that large disks are required $(R_d > 0.1R_{IC} \sim 10^{11}/T_6$ cm) and the low luminosities $(L_x \lesssim 10^{33}$ ergs s^{-1}, Córdova, Mason, and Nelson 1981) and efficiencies $(\epsilon \sim 10^{-3})$ imply that $\dot{M}_w/\dot{M}_a$ is small. On the other hand, in the case of accretion disks in quasars or active galactic nuclei, there is no binary to limit the disk size or to take up the angular momentum, so winds are likely to be an important mechanism for removing angular momentum over a wide range of parameters. The result in Figure 4 applies to such isolated disks as well.

Finally, we compare the effectiveness of winds with the other suggested mechanisms for angular momentum removal. Tidal interaction has been discussed above. Viscous interaction with a hot ambient medium (Gunn

1979) will dominate the wind only if its pressure exceeds p_0 so that the wind is suppressed. Since

$$p_0 = \frac{0.04 f\, T_{IC8}^2 (L/L_E)}{M_8\, \Xi_0'\, \xi^2}\ \text{ergs cm}^{-3}$$

$$= 0.027 f L_{46}/R_{18}^2\, \Xi_0'\ \text{ergs cm}^{-3} \qquad (4.22)$$

($M_8 = M/10^8\, M_\odot$) whereas the ambient gas is likely to have a pressure nearly independent of ξ, this will be possible only at very large radii. Magnetic fields (Blandford and Payne 1982) exert a torque $2R_0 B_z B_\phi/4\pi$. If we write $B_z B_\phi = (b/2)B^2$, where $b \leq 1$, then the wind carries off more angular momentum than the field if

$$p_0(Q_j/\xi) > b(B^2/8\pi)\,. \qquad (4.23)$$

(This condition is exact if $B \propto R_0^{-1}$ so that $B^2 \propto p_0 \propto R_0^{-2}$.) Since Q_j/ξ is typically of order unity, this is equivalent to requiring the gas pressure at the surface of the disk to exceed b times the magnetic pressure. Numerically, this condition becomes

$$B < 1.0 \left[\frac{f Q_j\, T_{IC8}^2 (L/L_E)}{M_8\, \Xi_0'\, b\xi^3}\right]^{1/2}\ \text{gauss}\,. \qquad (4.24)$$

No measurements of field strengths in accretion disks are available, so it is not clear whether this criterion is satisfied. We note that for binary X-ray sources, fields of order 10^4 gauss at a radius of order 10^{10} cm are required in order to dominate over the angular momentum loss due to the wind.

V. SUMMARY

In lieu of strong nonthermal heating from within the disk, the formation of a Compton-heated corona and wind above an accretion disk is inevitable if the photosphere of the disk is exposed to hard radiation from the central regions. The pressure at the base of the flow is proportional to the radiation intensity J reaching the base. Since this varies radially, the flow is strongly two-dimensional where the wind is strong, but we have shown that the mass loss rates are insensitive to the trajectories of the streamlines. Since we do not need to assume self-similarity to obtain an approximate map of the mass loss over the disk, our analysis is more general than that of Bardeen and Berger (1978), and we are able to consider all cases describing the relative importance of heating versus gravity. Our approximate two-dimensional analysis of the wind from the corona yields the surprising result that mass loss is significant down to radii where the inverse Compton temperature is only a tenth of the temperature necessary for escape from the gravitational field of the central body, since the large area of the sonic surface ($\sim 4\pi R_{IC}^2$) compensates for the pressure and density drop between the surface of the disk and the sonic surface.

In deriving our map of mass loss, we assume that the source of hard radiation is located in a compact region at the center of the disk. Nevertheless, radiation from this source can reach the photosphere of the opaque disk because the photosphere "flares" with radius. Flare is evident in the disk models of Shakura and Sunyaev

(1973), but even if it were absent there are other routes by which hard radiation could reach the surface of the disk. For example, if the X-ray source were extended (e.g., emission from the magnetic polar caps of a neutron star or emission from a pair of jets) or if the radiation from a compact source were scattered by material at high latitudes above the equatorial plane, then X-rays could "shine down" upon the disk. In Paper II we analyze the weakly flaring case; this represents a "least favorable" case in which a Compton-heated flow is possible, because the X-rays must traverse the corona/ wind along highly oblique paths in order to reach the base of the flow.

Compton-heated coronae and winds utilize only a small fraction of the energy available from the central X-ray source. This is true, in part, in the inner corona because the heated gas occupies a small solid angle as viewed from the source, and in the outer corona and wind because the optical depth through the flow is small (cf. Paper II). Furthermore, each scattering gives up only a fraction $kT/m_e c^2 \ll 1$ of the photon's energy, and relatively few photons are scattered more than once in the heated gas. As a result, there is not much one can infer about the relative importance of Compton heating in determining the thermal behavior of disk coronae and winds, compared with the various nonthermal mechanisms suggested by other authors (cf. § I). The energy flux in the latter is presumably limited to the local dissipation rate in the accretion disk, which is much smaller than the unattenuated X-ray flux from the central source; however, a much larger fraction of the available nonthermal energy may be absorbed by the gas.

Compton-heated winds lead to a mass loss from the disk $\dot{M}_w$ which is often comparable to or larger than the mass flow $\dot{M}_a$ onto the central object which produces the X-ray flux. Instability can result if $\dot{M}_w \gg \dot{M}_a$ since small fluctuations in L lead to small fluctuations in $\dot{M}_w$ which lead to large fluctuations in $\dot{M}_a$. This instability is the two-dimensional analog of the X-ray preheating instability in spherical accretion (Ostriker et al. 1976). The detailed behavior of the instability depends on the uncertain attenuation factor f, which will be estimated in Paper II. The instability can result in large-amplitude fluctuations in X-ray luminosity such as those observed in 4U 1626$-$67.

Compton-heated winds also remove angular momentum from the disk. If gas enters the disk with an angular momentum corresponding to a circular orbit at R_{in}, then mass loss from $R > R_{in}$ provides a sink for the angular momentum of the matter which accretes onto the central object. As a result, the disk is truncated at a radius $R_d > R_{in}$. For X-ray binaries in which mass is supplied to the disk through Roche lobe overflow, R_d may be smaller than that predicted by tidal truncation theories. Wind truncation requires $\dot{M}_w > \dot{M}_a$ and may be associated with the accretion instability described above. Since the excess angular momentum is lost to the system rather than being fed back into the orbit, the presence of a Compton-heated wind from the disk can influence the evolution of mass-transferring binaries.

Finally, we note that the momentum flux itself can have important dynamical consequences. Although the back pressure of the wind is generally small compared with the pressure inside the disk, so that it will not strongly modify the disk structure (Appendix B), the combination of static plus dynamic (ram) pressure in the wind will be enough to confine cool clouds in thermal equilibrium and at the ionization parameter inferred from the broad emission lines of quasars. Thus, Compton-heated winds can provide naturally the hot medium which must confine the broad-line emitting gas in quasars (KMT).

APPENDIX A

SELECTED GLOSSARY OF FREQUENTLY USED SYMBOLS

c_s	Isothermal sound speed
c_{IC}, c_{ch}	Isothermal sound speed at temperature T_{IC}, T_{ch}
F	Flux of radiation, measured at the source
f_g, f_{gs}	Form factor for effective gravity along streamline (eq. [3.7]), at adiabatic sonic point
f_Γ, f_{Γ_s}	Form factor for heating rate (eq. [3.9]), at adiabatic sonic point
$f_{\Gamma_0} \equiv f$	Attenuation factor (eq. [3.59]) = form factor for heating at base of corona/wind
h_d	Height of disk photosphere above midplane, effective thickness of disk
h'_d	Scale height of disk, may be smaller than h_d (eq. [4.11])
J, J^{ion}	Mean intensity of radiation integrated over all frequencies, from 1–10^3 rydbergs
J_0	Mean intensity of radiation at base of corona/wind (eq. [3.59])
$\tilde{j}$	Angular momentum per unit mass (eq. [4.12])
L, L^{ion}	Total luminosity, luminosity of ionizing radiation ($1 \leq h\nu \leq 10^3$ rydbergs)
L_E	Eddington limit
L_{cr}	Critical luminosity for wind parameter space (eq. [2.12])
M	Mass at center of accretion disk
$\dot{M}$	Local mass flux through disk
$\dot{M}_w$	Total mass loss rate due to wind (eq. [4.1])
$\dot{M}_{ch}$	Characteristic mass loss rate from disk (eq. [4.2])
$\dot{M}_a$	Accretion rate by central object
$\dot{M}_{in}$	Rate of mass injection into disk
$\dot{m}$	Mass loss per unit area of disk
$\dot{m}_{ch}$	$\equiv p_0/c_{ch}$ (eq. [3.12])
$\dot{m}^*$	$\equiv \dot{m}/\dot{m}_{ch}$ (eq. [3.12])
p_0	Gas pressure at base of corona/wind (eq. [3.60])
p^*, p_s^*, p_1^*	p/p_0 (eq. [3.11]), at adiabatic, isothermal sonic points
Q_m	Form factor for mass loss due to wind (eq. [4.3])
Q_j	Form factor for angular momentum loss due to wind (eq. [4.15])
R_0	Radius in plane of accretion disk
R_{IC}	Radius at which Compton temperature equals escape temperature (eq. [2.7])
R_{ch}	Radius at which wind barely is affected by gravity (eq. [2.11])
R_{iso}	Radius at which wind barely heats to Compton temperature (eq. [2.15])
R_d	Outer radius of disk; outer radius due to truncation by wind
R_{in}	Radius of circular orbit associated with gas injected into disk (eq. [4.19])
R_{max}	Radius at which orbits in Roche potential intersect (eq. [4.20])
r	Distance along streamline from disk surface; $r = R_0$ at surface
T_h	Equilibrium temperature of hot phase
T_{IC}	"Inverse Compton temperature", at which Compton heating balances inverse Compton cooling (eq. [2.4])

T_g	"Escape temperature" $\equiv GM\mu/R_0 k$
T_{ch}	"Characteristic temperature" of steadily heated wind (eq. [2.9])
T^*, T_s^*, T_1^*	$\equiv T/T_{ch}$ (eq. [3.11]), at adiabatic, isothermal sonic points
y	$\equiv r/R_0$, dimensionless distance along streamline (eq. [3.1])
y_s, y_1	Adiabatic (eq. [3.17]), isothermal (eq. [3.18]) sonic point
α	$\equiv (T_{ch}/T_g)^{1/2}$, measures ability of wind to heat to escape temperature in free fall time (eq. [2.10])
α_d	"Alpha-parameter" of standard accretion disk theory (Shakura and Sunyaev 1973)
β	Exponent describing divergence of streamlines (eq. [3.3])
$\langle\beta\rangle$	Log-weighted average of β
β_s, β_1	β at adiabatic (eq. [3.17]) and isothermal (eq. [3.18]) sonic points
Γ	Heating rate
Γ_0	Optically thin heating rate at R_0
ϵ	Efficiency of mass-to-energy conversion in the accretion flow (eq. [4.6])
ϵ_{-1}	$\equiv \epsilon/0.1$
η, η_s	Defined eq. (3.20), evaluated at adiabatic sonic point (eq. [3.22])
μ, μ_e	Mean mass per particle, per free electron
$\tilde{\mu}$	Mass ratio of compact X-ray source to total mass of binary
Ξ'	Ionization parameter; for a beam of radiation, ratio of radiation pressure to gas pressure (eq. [2.1])
Ξ	Ionization parameter used by KMT, $= (2.3J^{ion}/J)\Xi'$
$\Xi'_{c,max}$	Maximum Ξ' allowing gas in cool phase
$\Xi'_{h,min}$	Minimum Ξ' allowing gas in hot phase
Ξ'_0	Ξ' at base of corona/wind (eq. [3.60])
ξ	$\equiv R_0/R_{IC}$ (eq. [2.8]); in general, $\xi_x = R_x/R_0$
Σ	Surface density of disk (eq. [B.3a])

APPENDIX B

HEIGHT OF AN X-RAY HEATED ACCRETION DISK

In our analysis of mass and angular momentum loss from accretion disks in § IV, we assumed that the height of the disk was fixed. Here we show that in practice this assumption is generally satisfied: h_d is only weakly dependent on the surface density Σ or the luminosity. We also discuss the modifications in disk structure associated with a Compton-heated corona and wind.

Radiation from the central source and the inner parts of the disk heats and thickens the outer regions of the disk (Cunningham 1976). Over much of the surface of a disk around a high-efficiency source ($\epsilon \gg 10^{-3}$), such external heating dominates local viscous energy dissipation (Cunningham 1976; Paper II). A corona or wind can alter these effects in several ways: first, the radiation is generally absorbed at the interface between the disk and the corona or wind ($h = h_d$), where the pressure is p_0 (eq. [3.60]). As we shall see, h_d is typically related to the scale height h'_d by $h_d \sim (2-3)h'_d$. Second, this disk can in principle become pressurized by the wind, so that $h_d \lesssim h'_d$; however, this occurs at such large radii ($\xi \gtrsim 100$) that other effects are likely to intervene. Finally, the corona and wind can scatter X-rays down onto the disk (see Paper II), thereby increasing the effective temperature above that given by direct irradiation alone.

Following Cunningham (1976), we model the disk as being isothermal in the vertical direction, a reasonably good approximation for standard α-model disks (Shakura and Sunyaev 1973) and an even better approximation for externally heated disks. An isothermal disk has a pressure

$$p = p_c \exp\left[-(h/h'_d)^2\right], \tag{B1}$$

where the scale height is given in terms of the isothermal sound speed in the disk c_s by

$$h'_d = 2^{1/2}(c_s/v_\phi)R_0 . \tag{B2}$$

Cunningham (1976) assumed that the disk was unbounded vertically, and made the approximation that the radiation was absorbed at one scale height ($h = h'_d$) above and below the midplane. In fact, the disk is generally highly opaque and, as remarked above, the radiation is absorbed at $h = h_d$ where $p = p_0$.

The surface density of the disk is

$$\Sigma = \int_{-h_d}^{h_d} \rho\, dh \tag{B3a}$$

$$= \frac{\pi^{1/2} p_c h'_d}{c_s^2} \operatorname{erf}\left(\frac{h_d}{h'_d}\right) , \tag{B3b}$$

where erf (x) is the error function. Let p_{cu} be the pressure in the midplane of an unbounded disk, i.e., one in which $p_0 = 0$ as assumed by Cunningham. For such a disk erf (h_d/h'_d) = erf (∞) = 1 and we have

$$p_{cu} = \Sigma c_s^2/\pi^{1/2} h'_d . \tag{B4}$$

Equations (B1), (B3b), and (B4) then provide two simultaneous equations for the unknowns p_c (the actual central pressure) and h_d:

$$p_c = p_{cu}/\text{erf } (h_d/h'_d) = p_0 \exp (h_d/h'_d)^2 . \tag{B5}$$

These equations can be solved in the limiting cases of small surface pressure

$$\frac{h_d}{h'_d} \approx \left[\ln \frac{p_{cu}}{p_0}\right]^{1/2} \propto (\ln \Sigma)^{1/2} , \tag{B6}$$

$$p_0 \ll p_{cu} \approx p_c ; \tag{B7}$$

and large surface pressure

$$\frac{h_d}{h'_d} \approx \frac{\pi^{1/2}}{2} \frac{p_{cu}}{p_0} \propto \Sigma , \tag{B8}$$

$$p_{cu} \ll p_0 \approx p_c . \tag{B9}$$

An approximate solution for h_d/h'_d which has an accuracy of 5% over the entire range of p_0/p_{cu} is

$$\frac{h_d}{h'_d} \simeq \left[\ln \left(1 + \frac{\pi}{2} \frac{p_{cu}^2}{p_0^2}\right)^{1/2}\right]^{1/2} . \tag{B10}$$

Note that in the case of small surface pressure ($p_0 \ll p_{cu}$; eq. [B6]) the height of the disk h_d is insensitive to the surface density Σ. We now demonstrate that this is usually the case in practice.

To this point our discussion has been independent of the uncertain viscosity in the disk. In order to relate Σ to observable quantities, however, we adopt an α-model disk (Shakura and Sunyaev 1973) in which

$$\dot{M}(\xi) = 2\pi\alpha_d c_s h'_d \Sigma . \tag{B11}$$

This relation is not significantly altered by mass loss (Liang and Price 1977). The vertical electron scattering optical depth through the disk is

$$\tau_{es} = \Sigma \sigma_T/\mu_e \tag{B12}$$

$$= \frac{780(L/L_E)}{\alpha_d \epsilon_{-1} T_{d4}} \frac{\dot{M}(\xi)}{\dot{M}_a} \left(\frac{T_{IC8}}{\xi}\right)^{3/2} , \tag{B13}$$

where we have used equations (4.6) and (B2). The quantity T_{d4} is the disk temperature in units of 10^4 K, and is typically of order unity for $\xi \sim 1$ (Cunningham 1976; Paper II). If θ_i is the angle of incidence for the external irradiation, then we require $\tau_{es}/\cos \theta_i \gg 1$ in order to ensure that the hard X-rays are absorbed near the surface of the disk ($h \sim h_d$). Since $\dot{M}(\xi) = \dot{M}_a + \dot{M}_w(\xi) > \dot{M}_a$, equation (B13) shows that this will generally be true unless the luminosity is very low.

The ratio of the central pressure of an unbounded disk to p_0 varies as Σ just as τ_{es} does. Equations (3.60), (4.6), and (B4) yield

$$\frac{p_{cu}}{p_0} = 2.2 \frac{\dot{M}(\xi)}{\dot{M}_a} \frac{T_{IC8} \Xi'_0}{\alpha_d \epsilon_{-1} f T_{d4}^{1/2} \xi} . \tag{B14}$$

This ratio is almost always large. In the inner parts of the disk ($\xi \lesssim 0.1$), we have $\dot{M}(\xi) \approx \dot{M}_a$ and

$$\frac{p_{cu}}{p_0} = 22.0 \frac{T_{IC8} \Xi'_0}{\alpha_d \epsilon_{-1} f T_{d4}^{1/2}} \left(\frac{0.1}{\xi}\right) ; \tag{B15}$$

in Region A + E ($\xi > 0.1$) we have $\dot{M}(\xi) > \dot{M}_w(\xi)$ so that

$$\frac{p_{cu}}{p_0} \geq \frac{28}{\alpha_d} \left(\frac{T_{IC8}}{T_{d4}}\right)^{1/2} \frac{\ln (12.5\xi)}{\xi} . \tag{B16}$$

In the remaining regions the ratio is larger yet. Hence the surface pressure is small ($p_0 \ll p_{cu}$) except at very large radii, $\xi \gtrsim 100/\alpha_d$. So long as the surface pressure is small, equations (B6)–(B9) imply that the height of the disk is insensitive to the surface density Σ. This means that moderate changes in Σ, such as those caused by the onset of the

wind-driven instability discussed in § IVa, will only weakly affect the transfer of X-rays to the surface of the disk. Since the scale height varies as $T_d^{1/2}$, which in turn varies as $L^{1/8}$, the disk height is insensitive to variations in L as well. (A similar scaling, with different normalization, holds for radiation generated within the disk itself.) Therefore, for most disks the height of the disk is insensitive to variations in the mass of the disk or in the central luminosity.

REFERENCES

Arons, J. 1973, *Ap. J.*, **184**, 539.
Balbus, S. A., and McKee, C. F. 1982, *Ap. J.*, **252**, 529.
Bardeen, J. M., and Berger, B. K. 1978, *Ap. J.*, **221**, 105.
Bardeen, J. M., and Petterson, J. A. 1975, *Ap. J. (Letters)*, **195**, L65.
Begelman, M. C., and McKee, C. F. 1983, *Ap. J.*, **271**, 89 (Paper II).
Blandford, R., and Payne, D. 1982, *M.N.R.A.S.*, **199**, 883.
Bisnovatyi-Kogan, G. S., and Blinnikov, S. I. 1977, *Astr. Ap.*, **59**, 111.
Castor, J. I., Abbott, D. C., and Klein, R. I. 1975, *Ap. J.*, **195**, 157.
Córdova, F. A., Mason, K. O., and Nelson, J. E. 1981, *Ap. J.*, **245**, 609.
Cowie, L. L., Ostriker, J. P., and Stark, A. 1978, *Ap. J.*, **226**, 1041.
Cunningham, C. 1976, *Ap. J.*, **208**, 534.
Davidson, K., and Ostriker, J. P. 1973, *Ap. J.*, **179**, 585.
Flannery, B. P. 1975, *M.N.R.A.S.*, **170**, 325.
Galeev, A. A., Rosner, R., and Vaiana, G. S. 1979, *Ap. J.*, **229**, 318.
Gunn, J. E. 1979, in *Active Galactic Nuclei*, ed. C. R. Hazard and S. Mitton (Cambridge: Cambridge University Press), p. 213.
Icke, V. 1976, in *IAU Symposium 73, The Structure and Evolution of Close Binary Systems*, ed. P. Eggleton, S. Mitton, and J. Whelan (Dordrecht: Reidel), p. 267.
Krolik, J. H., and London, R. 1983, *Ap. J.*, **267**, 18.
Krolik, J. H., McKee, C. F., and Tarter, C. B. 1981, *Ap. J.*, **249**, 422 (KMT).

Li, F. K., Joss, P. C., McClintock, J. E., Rappaport, S., and Wright, E. L. 1980, *Ap. J.*, **240**, 628.
Liang, E. P. T., and Price, R. H. 1977, *Ap. J.*, **218**, 247.
Liang, E. P. T., and Thompson, K., 1979, *M.N.R.A.S.*, **189**, 421.
Livio, M., and Shaviv, G. 1981, *Ap. J.*, **244**, 290.
London, R. A., and Flannery, B. P. 1982, *Ap. J.*, **258**, 260.
London, R. A., McCray, R., and Auer, L. 1981, *Ap. J.*, **243**, 970.
McCray, R. A., Shull, J. M., Boynton, P. E., Deeter, J. E., Holt, S. S., and White, N. E. 1982, *Ap. J.*, **262**, 301.
Middleditch, J., Mason, K. O., Nelson, J. E., and White, N. E. 1981, *Ap. J.*, **244**, 1001.
Ostriker, J. P., McCray, R., Weaver, R., and Yahil, A. 1976, *Ap. J. (Letters)*, **208**, L61.
Paczyński, B. 1977, *Ap. J.*, **216**, 822.
———. 1978, *Acta Astr.*, **28**, 91.
Petterson, J. A. 1977, *Ap. J.*, **218**, 783.
Roberts, W. J. 1974, *Ap. J.*, **187**, 575.
Shakura, N. I., and Sunyaev, R. A. 1973, *Astr. Ap.*, **24**, 337.
Shu, F. H., and Lubow, S. H. 1981, *Ann. Rev. Astr. Ap.*, **19**, 277.
Smak, J. 1976, *Acta Astr.*, **12**, 28.

M. C. BEGELMAN: Joint Institute for Laboratory Astrophysics, University of Colorado, Boulder, CO   80309

C. F. McKEE: Department of Physics, University of California, Berkeley, CA   94720

G. A. SHIELDS: Department of Astronomy, University of Texas, Austin, TX   78712